4-18-2017 12:00 AM

# Effective Boronizing Process for Age Hardened Inconel 718

Aria Khalili, *The University of Western Ontario*

Supervisor: Dr. Robert J. Klassen, *The University of Western Ontario*

A thesis submitted in partial fulfillment of the requirements for the Master of Engineering Science degree in Mechanical and Materials Engineering

## Abstract

Boronizing or boriding is a technique to mitigate wear damage in industrial valves made of age-hardenable Inconel® 718 which is a nickel-based superalloy. Boriding involves immersing the part in a patented boron-based compound and heating over 800 °C.

Boriding combined with aging has a detrimental thermal effect and was the subject of this investigation. The effects on hardness, wear and grain size, of boriding and aging separately, subsequently, and simultaneously, were investigated to observe the microstructure and mechanical properties.

The results show that boriding has negligible effect on the grain size and the hardness of the substrate. Besides, a boride coating can improve the surface hardness by a factor of five and reduce the wear damage by over 75%. As the wear performance strongly depends on the coating thickness, we found that initial aging and subsequent boriding delivers the thickest layer and is the best method for boriding of Inconel® 718.



## Keywords

Pack Boriding, Inconel® 718, Ekabor® Ni, Aging, Coating, Wear Resistance, Superalloy, Microhardness, Nanohardness.

*To Maman and Baba*

# Acknowledgments

I wish to express my gratitude to Dr. Robert J. Klassen, my supervisor and professor. Being accepted as a student of Dr. Klassen and working in his group has been an exceptional honour and a great experience in my academic life. I am grateful for his expert guidance and the motivation he provided throughout this project, especially at those frustrating times when I felt deadlocked.

Dr. Klassen's research group over the past three years has stimulated me in this project and I would like to extend my sincere thanks to them: Dr. Vineet Bhakhri, Dr. Meysam Haghshenas, Dr. A. Z. M. Ariful Islam, Heygaan Rajakummar, Md. Imran Khan, Maisaa Tawfeeq, Feifei Nie, Mahdi Bagheripoor and Lobat Shojaei.

I am thankful for the help and direction from my mentor and friend, Dr. Mehdi Yari at Surface Heat Treat and Coatings in Hamilton, whom I have known since my undergraduate years at Azad University in Tehran, and whom has continuously supported me. A special thanks to the CEO of Surface Heat Treat and Coatings, Mr. John Abrahamse, for allowing me to use their facilities.

Significant parts of this project were done in the laboratories of my advisors, Dr. Jeffrey T. Wood and Dr. X. A. (Andy) Sun. I am grateful for their advice and for permission to use their facilities. I also thank Marc Beauchamp in the Department of Earth Sciences for assisting me in using their scanning electron microscope (SEM).

I acknowledge the help of many wonderful people in the MME department, especially Chris Seres, Joanna Blom and Claire Naudi, and support from the Machine Shop, Clayton Cook and Steve Concannon. Rest in peace Steve; you are always in my memory.

Last but not least, many thanks to all my friends and family who supported me through the happy and the rough days: Robert Swartman, Toba Mohabbati, Morteza Malekmanesh, Maryam Ghahremani, Megaraja Elayathamby, Pouria Khalili, Afshan Samani, Pouya Sharifi, Anibran Banerjee, Babak Razaghi Rad, Elnaz Nouri, Anahita Nouri and my parents, Noor and Fereydoun.

# Table of Contents

# List of Tables

# List of Figures

# Acronyms

| | |
|---|---|
| AB | Aged Boronized |
| APB | Anti-Phase Boundary |
| ASM | American Society for Metals |
| ASTM | American Society for Testing and Materials |
| BA | Boronized Aged |
| Bal. | Balance |
| BSE | Back Scattered Electron |
| CVD | Chemical Vapor Deposition |
| C.Z. | Compound Zone |
| D.Z. | Dispersed Zone |
| Eq. | Equation |
| FBT | Fluidized Bed Technology |
| FCC | Face Center Cubic |
| G.B.Z. | Grain Boundary Zone |
| JA | Just Aged |
| JB | Just Boronized |
| Max. | Maximum |
| Min. | Minimum |
| PVD | Physical Vapor Deposition |
| ® | Registered Trademark Symbol |
| RT | Room Temperature |
| SAB | Simultaneously Aged Boronized |
| SAE | Society of Automotive Engineers |
| SEM | Scanning Electron Microscope |
| SPS | Spark Plasma Sintering |
| TEM | Transmission Electron Microscope |
| Temp. | Temperature |
| TBC | Thermal Barrier Coating |
| UNS | Unified Numbering System |
| UTS | Ultimate Tensile Strength |
| WDS | Wavelength Dispersive Spectroscopy |
| XRD | X-Ray Diffraction |

# Symbols

| | |
|---|---|
| $2\theta$ | X-ray Diffraction Degree |
| A | Surface Area |
| $A_p$ | Projected Area |
| a | Lattice Parameter |
| $a_o$ | Lattice Parameter |
| $\alpha$ | Coefficient of Expansion |
| b | Lattice Parameter |
| c | Lattice Parameter |
| $c$ | Concentration |
| $\gamma$ | Ni Austenite phase |
| $\gamma'$ | $Ni_3(Ti, Al)$ Face Center Cubic Phase |
| $\gamma''$ | $Ni_3Nb$ Body Center Tetragonal Phase |
| D | Diffusion Coefficient |
| $d$ | Diameter |
| $\delta$ | $Ni_3Nb$ Orthorhombic Phase |
| E | Modulus of Elasticity |
| $\varepsilon$ | Strain |
| F | Force (Loading) |
| $\eta$ | $Ni_3Ti$ Hexagonal Close Packed Phase |
| $h_p$ | Indentation Depth |
| HV | Hardness Vickers |
| $I_{(100, \%)}$ | X-ray Diffraction Intensity |
| $i$ | $i$th Species |
| L | Liquid |
| $\lambda$ | Wave Length |
| M | Metal |
| m | Monoclinic |
| $M_w$ | Molecular Weight |
| $\mu$ | Coefficient of friction |
| o | Orthorhombic |
| $R$ | Universal Gas Constant |
| $\rho$ | Density |
| $r$ | Atom Radius |
| $r_B$ | Radius of Boron Atoms |
| S | Solid |
| $\sigma$ | Tensile Stress |
| $\sigma$ | Fe-Cr, Fe-Cr-Mo Tetragonal Phase |
| $\sigma_y$ | Yield Stress |
| $\sigma_{uts}$ | Ultimate Tensile Strength Stress |
| $T$ | Temperature |
| $t$ | Time |
| wt.% | Weight Percent |
| $x$ | Position |

# Chapter 1

## 1 INTRODUCTION

The Industrial revolution (1760-1840) was a transformative time in Europe when new types of metal alloys, particularly steel alloys, were developed with suitable chemical composition to provide the high mechanical strength required for use in elaborate new machinery such as engines, automobiles, and shipping. Subsequent development of more elaborate equipment required alloys with even higher mechanical strength and resistance to elevated temperature and aggressive corrosive environments. As a result, new "stainless steel" alloy grades containing large additions of chromium were developed in the decade between 1910 and 1920. While the early stainless steel alloys represented a tremendous improvement in general corrosion resistance, their mechanical strength, particularly at high temperature, was modest. During the second world war, however, the strength and high temperature performance of stainless steels was improved tremendously by the addition of alloying elements such as cobalt. These were referred to as "super-alloys". In the following years several classes of superalloys were developed and nickel-based superalloys are currently the most commonly used [1].

The Inconel® 718 has the most applications among nickel-based superalloys. This alloy is, as a rule, used in the age-hardened condition which provides it with high strength up to a temperature of about 550 $^{o}$C. One area of weakness of superalloys, like Inconel® 718, is their unsatisfactory resistance to abrasion (wear). A standard method to mitigate this is to apply a hard surface coating to the alloy [2].

Boronizing is a case-hardening method which provides a hardened surface layer of up to several hundred micrometers thickness. Within this layer the boron atoms harden the substrate by either solid-solution hardening or formation of intermetallic boride precipitates. A boriding process has been developed for Ni-based alloys where surface hardening is achieved by the precipitation of Ni-B intermetallics. While this technique has been demonstrated to provide a hard surface that is stable up to about 850 $^{o}$C it has, as of yet, not been used for the most common Ni-based superalloy, Inconel® 718, primarily

because the conventional boriding thermal treatment negatively affects the age hardening of the alloy.

The objectives of this thesis are to research the effect of the boriding thermal process on the age hardening of the Inconel® 718 alloy and to formulate an optimal set of thermal treatments that will allow this important alloy to be borided while still retaining its age hardened mechanical strength.

This thesis is composed of six chapters. Chapter 2 discusses the properties and microstructure of Inconel® 718 and the procedure by which Ni-based alloys are pack-borided. Chapter 3 describes the experimental procedures followed in this research and includes a detailed description of the Inconel® 718 test material, the Ekabor® Ni boriding process, the microstructural analyses performed, the micro-indentation hardness testing, and the pin-on-disk wear testing performed. Chapter 4 presents the results of the experiments. Chapter 5 provides a discussion of the results. Chapter 6 presents the conclusions drawn from the experiments performed, discusses their significance, and suggests topics for future studies to carry on from this research.

# Chapter 2

# 2 LITERATURE REVIEW

The objective of this thesis is to assess the effect of a boronizing surface-hardening process on the indentation hardness and wear resistance of the Inconel® 718 superalloy and to determine if a convenient method exists to boronize this alloy in its age hardened condition. To place this research into proper perspective this chapter reviews the background information related to age hardened Inconel® 718 and the boronizing process.

## 2.1 Inconel® 718 Superalloys

Inconel® 718 is an austenitic nickel-based alloy of composition shown in Table 2.1 [3-4].

**Table 2.1: Chemical composition range of the Inconel® 718 nickel base superalloy [3].**

| Element (wt. %) | Ni | Cr | Nb | Mo | Ti | Co | Al | Mn | Si | Cu | C | Ta | S | P | B | Pb | Se | Bi | Fe |
|---|---|---|---|---|---|---|---|---|---|---|---|---|---|---|---|---|---|---|---|
| ***Min.*** | 50 | 17.0 | 4.75 | 2.80 | 0.65 | 0 | 0.20 | 0 | 0 | 0 | 0 | 0 | 0 | 0 | 0 | 0 | 0 | 0 | Bal. |
| ***Max.*** | 55 | 21.0 | 5.50 | 3.30 | 1.15 | 1 | 0.80 | 0.35 | 0.35 | 0.3 | 0.08 | 0.05 | 0.015 | 0.015 | 0.006 | 0.0005 | 0.0003 | 0.00003 | |

The alloy is used almost exclusively in the age hardened condition where it is significantly strengthened by the precipitation of both $Ni_3(Al, Ti)$ γ' and $Ni_3Nb$ γ" precipitates [5-7]. Fig. 2.1 (a) displays the Time-Temperature-Transformation (TTT) diagram of Inconel® 718 and illustrates the time necessary to precipitate the γ' and γ" phases by isothermal aging [8]. The standard aging heat treatment for the Inconel® 718 alloy is described in SAE AES 5663M and ASTM A 1014-03 [4-5, 9-10] and is shown in Fig. 2.1 (b). The heat treatment begins by solution annealing the material at 941 to 1010 ºC to establish a single phase FCC γ crystal structure [1]. The first isothermal aging step is performed at 718 to 760 ºC for 8-hour duration [4]. During this stage both γ' and γ" phases precipitate and grow rather rapidly to form relatively large, but still coherent, precipitates [11]. The sample is then cooled to a temperature of 621 to 649 ºC and, once again, held for 8 hours [4]. During this stage a distribution of smaller coherent γ' and γ" precipitates are nucleated [11].

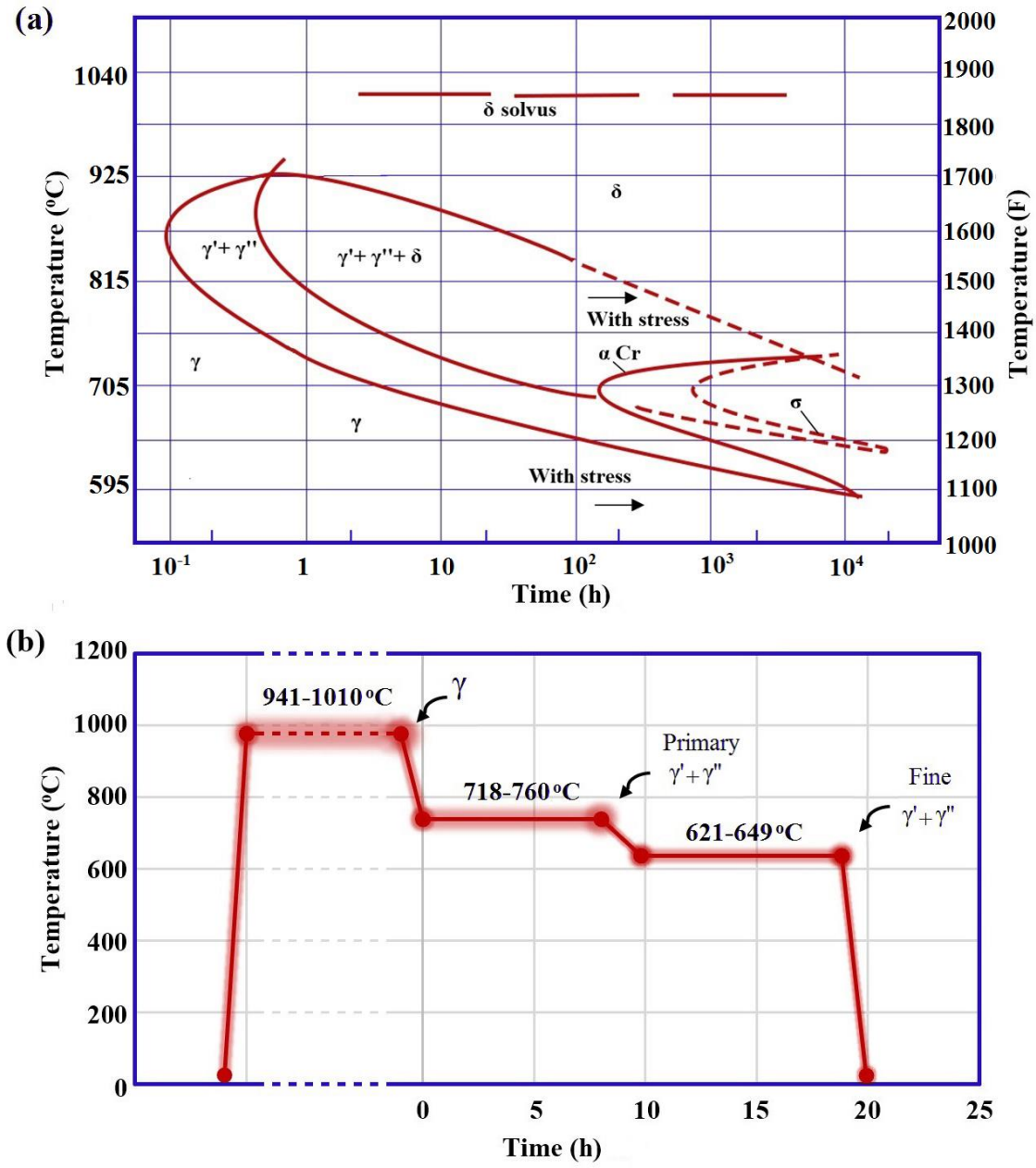


**Figure 2.1: (a) Time Temperature Transformation (TTT) diagram of the Inconel® 718 alloy. (b) Standard Temperature Time profile used in the isothermal age hardening of Inconel® 718 (adapted from [4, 8-10]).**

Fig. 2.2 (a) and (b) shows the resulting microstructure [12-13]. These images illustrate the small size of the γ'- γ" precipitates in the age hardened Inconel® 718. The γ" precipitates are uniformly distributed and disc-shaped with diameter in the ten to hundred angstrom range [1, 14]. The precipitates give this alloy exceptionally good ambient temperature

mechanical strength ($\sigma_{yield} \approx 1034$ MPa and $\sigma_{ultimate} \approx 1276$ MPa) [9]. Other alloying elements also contribute to the strength of the Inconel® 718 alloy by forming additional incoherent carbides ($M_{23}C_6$, $M_6C$, $M_7C_3$) where the metal M can be Cr, Mo, Nb, Ta or Ti [14].

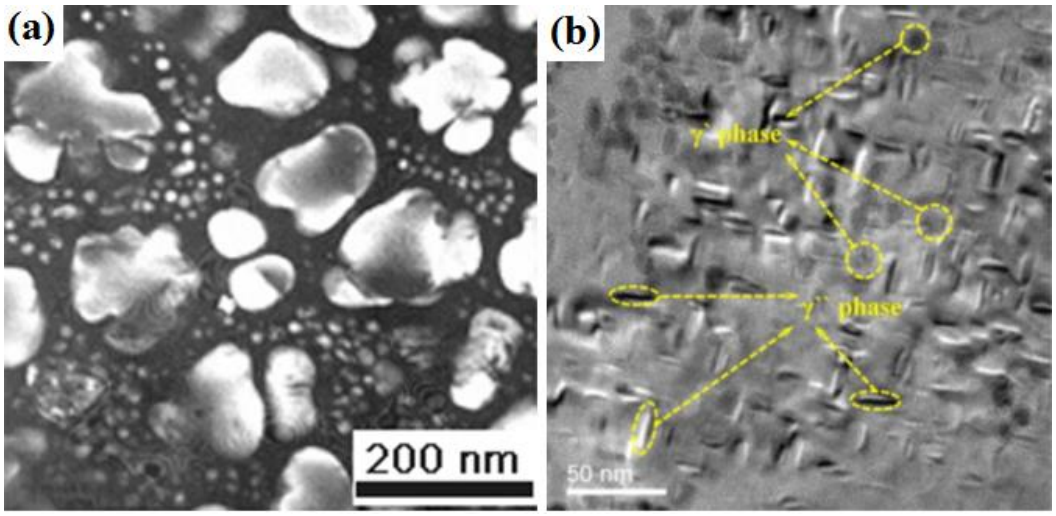


**Figure 2.2: TEM images of (a) coarser and finer γ' as a result of two stage heat treatment and (b) γ' and γ'' in Inconel® 718 after solution treatment and aging [12-13].**

Age hardening of the Inconel® 718 is accomplished by the precipitation of coherent $Ni_3Nb$ γ'' precipitates. To promote this the alloy has a high Nb content and is referred to as a "Niobium-modified Inconel". The diffusivity of Nb within this alloy is quite slow, owing primarily to its large atomic size, thus the γ'' precipitates in the age hardened Inconel® 718 are very thermally stable leading to this alloy's exceptionally good high temperature strength (Fig. 2.3) [14].

### 2.1.1 Wear of Inconel® 718

One notable weakness of the Inconel® 718 alloy is its mediocre resistance to abrasive wear [15]. The passive surface oxide layer formed on this alloy is vulnerable to break down during severe abrasion [16]. The exposed metal has a very high coefficient of friction resulting in the increased possibility of galling, seizing or fretting wear [17-18]. As a result,

improvement of surface properties of the Inconel® 718 alloy is necessary to improve its usefulness. This can be achieved by applying a hard surface coating as described below.

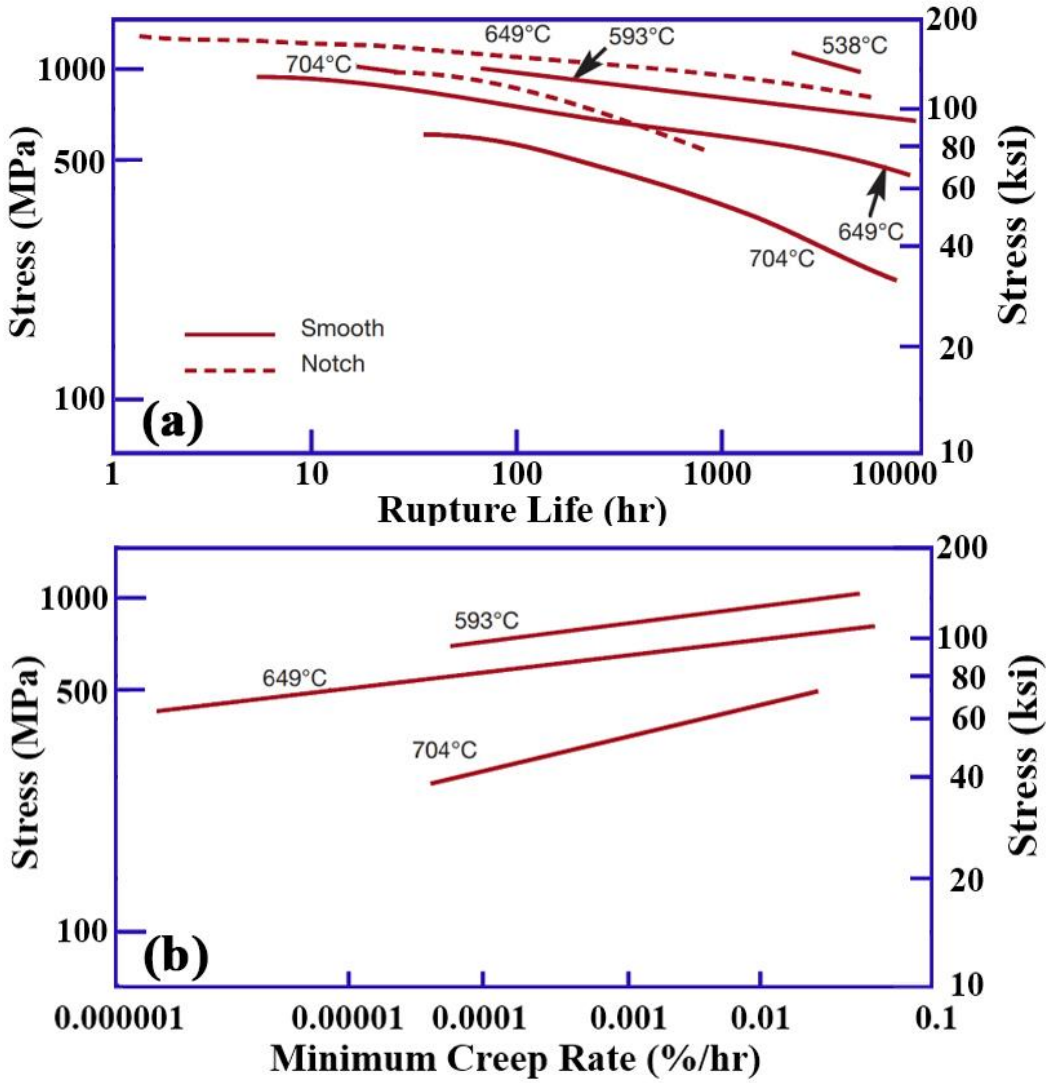


**Figure 2.3: Creep behaviour of age hardened Inconel® 718; (a) rupture life and (b) creep rate at various stresses and temperatures (adapted from [5]).**

## 2.2 Surface Coatings for Inconel® 718

There are two general types of coatings used to improve the high temperature performance of alloys; physical overlays and diffusion coatings.

### 2.2.1 Physical Overlays

A physical overlay is a ceramic or intermetallic surface coating applied by a process such as chemical vapor deposition (CVD), physical vapor deposition (PVD), thermal spraying, or cladding [7, 17]. The adhesive strength of these overlays is obtained primarily by interatomic bonding of the overlay material within the first several atom layers of the substrate. No significant atomic interdiffusion occurs between the overlay and the substrate. A very common type of physical overlay used for protecting metal surfaces are nitride compounds such as TiN, ZrN, or CrN. These nitride overlays are commonly applied by PVD techniques to Inconel® 718 gears, bearings, and ball valves [17]. Another example of this sort of coating for superalloys are intermetallic (Ni, Mo) CrAlY thermal barrier coatings (TBCs) [7]. These physical overlays are completely chemically and crystallographically different than the substrate alloy. As a result, the overlay/substrate interfacial bond strength is often quite low leading to the potential for interfacial failure and spalling off of the overlay during service. This becomes particularly problematic when the thickness of the physical overlay is increased. The typical thickness of such overlays is thus usually less than about 2 μm.

Studies have demonstrated that the physical overlay coatings are effective in reducing abrasion damage. In fact, they are frequently used in gas turbine engines to mitigate corrosion and erosion deterioration in the high temperature aggressive environment. J. A. Sue and T. P. Chang reported that a 6 to 8 μm thick overlay of TiN, ZrN or CrN can improve the wear resistance by 10, 100, 1000 times respectively at 500 $^{o}$C [19]. In wear condition, the thicker the protective layer the longer the life time of the component. Unfortunately, as discussed previously, thick physical overlay coatings suffer from increased internal residual stress resulting in decreased interfacial bond strength and this ultimately limits the extent that they can improve a metal's wear resistance. Moreover, the materials and procedure for this type of coatings are costly, limiting their application to high-tech industries such as aerospace [7, 20]. A tactic to tackle the adhesion problem as well as increasing the load tolerance and modify crack propagation rate is to produce a multilayer system by depositing successive layers of overlay coatings [21-23]. Fig. 2.4 illustrates the effectiveness of thick Cr/CrN multilayer coatings on improving the wear

resistance of Inconel® 718. While thin physically deposited multilayers are very promising in improving the wear resistance, the deposition time and the associated cost of these coatings is very high [17].

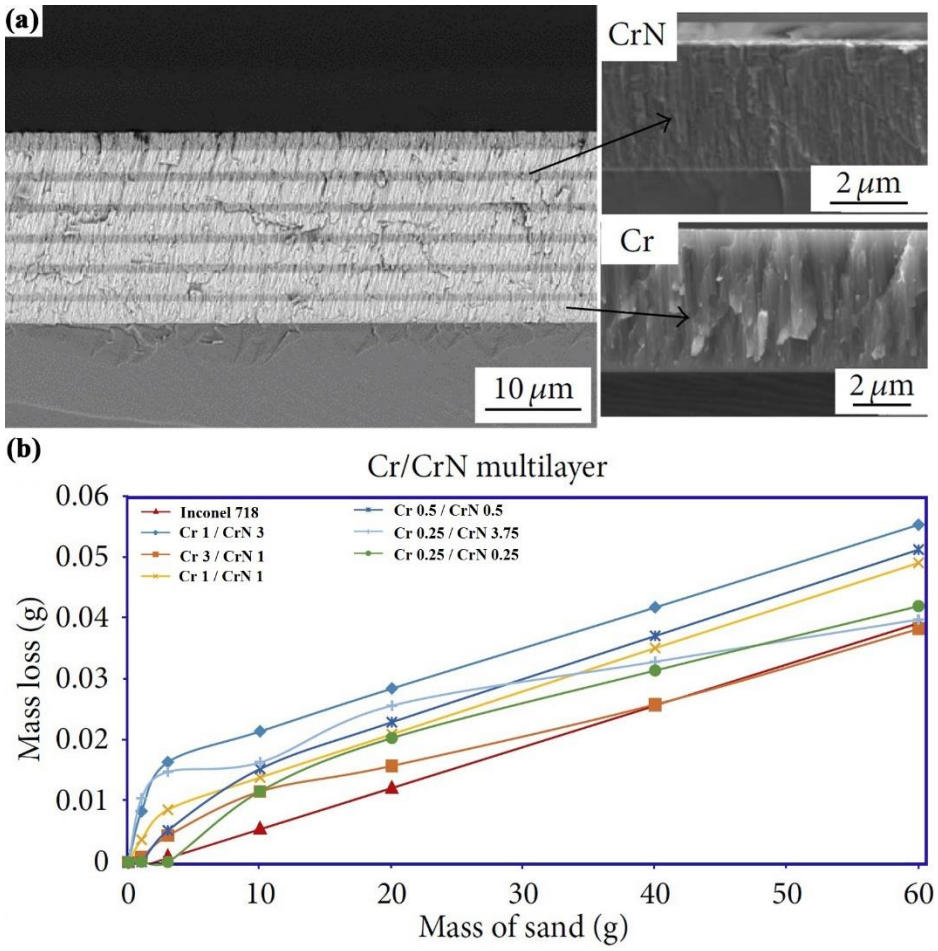


**Figure 2.4: (a) Multilayer coating of Cr/CrN on an Inconel® 718 substrate. (b) Erosion resistance of the coating when subjected to bombardment with SiC particles (adapted from [24]).**

## 2.2.2 Diffusion Coatings

Hard surfaces are commonly made on metal structures through a process that involves solid-state diffusion of an alloying element into the metal. This technique is relatively easy to perform and can invoke significant alloy element diffusion to depths up to about 100 μm. Depending upon the alloy element used, significant solid-solution and/or precipitation strengthening can be achieved within the diffusion zone. In addition, the

chemical composition of the material in the diffusion zone ensures a gradient in interatomic spacing which reduces the inter-atomic mismatch strains within the diffusion zone. This reduces the chance for adhesive failure of the material within the hardened diffusion zone from the substrate and results in a hardened layer that is more resistant to abrasive wear [17].

Numerous diffusion coating techniques have been developed over the last century but the oldest, and still the most commonly used, is the pack or solid cementation process. In this process the diffusing agent is in form of a powder composed of three components; i) the metal powder to be diffused into the substrate, ii) a halide compound that facilitates the diffusion process, and iii) a filler material that controls the kinetics of the diffusion process. The material to be surface hardened is embedded in the agent powder and is heated up to the diffusion temperature. At this temperature, the halogen-carrying compound decomposes, and the halogen part forms a metal halide gas with the metal that is to be diffused into the substrate. When this gas adsorbs on the surface of the substrate it releases the metal atoms and the halogen part then returns to its original activator composition to repeat its task of transferring metal atoms [7]. Fig. 2.5 summarizes this mechanism.

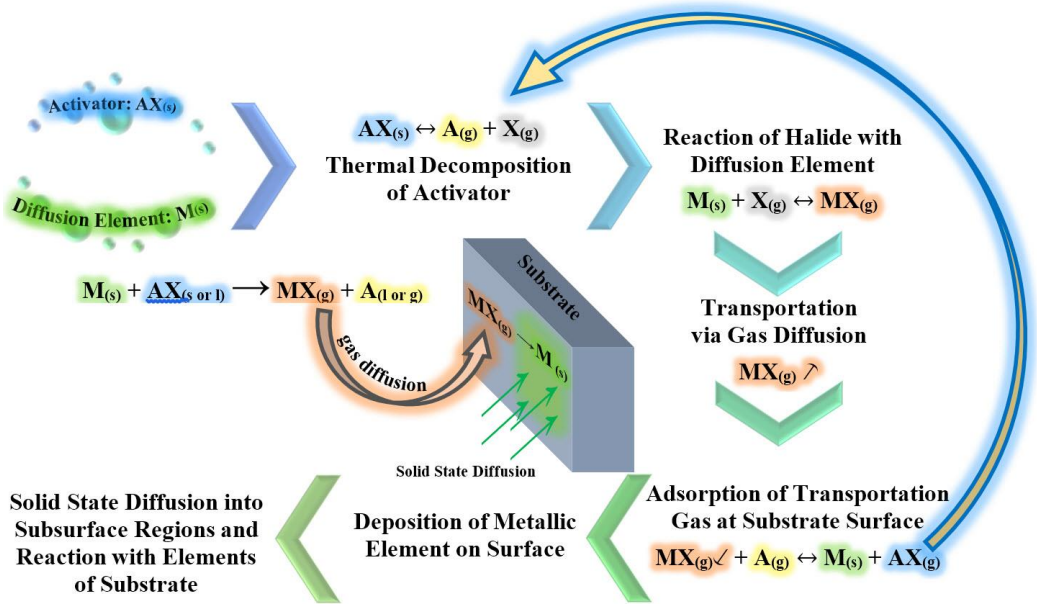


**Figure 2.5: General mechanism of pack cementation (adapted from [7]).**

This technique for making diffusion coatings is frequently applied to create carbon, nitrogen, and/or boron diffusion hardened layers on steel alloys [25]. Nonetheless, carburizing and nitriding are not ideal for nickel alloys because of the very limited solubility of carbon and nitrogen in nickel [15, 25]. Boron, on the other hand, forms extensive strongly bonded intermetallic compounds with nickel and this results in significantly improved diffusion coatings. The life of boride diffusion layers is more than twice that of carbide or nitride diffusion layers on Ni-based alloys subjected to intense abrasive wear loadings [25].

#### 2.2.2.1 Boride Diffusion Layers on Nickel Bearing Alloys

Solid or pack boronizing of nickel bearing alloys is very attractive because of the simplicity of the technique, the unsophisticated equipment required, and its cost-effectiveness [26-27]. The boriding powder, consisting of a boriding agent, halogen activator and filler, is packed around a workpiece in a steel container and is heated up to between 700 and 1100 $^{o}$C in a furnace with controlled atmosphere (nitrogen, helium or argon) for 3 to 16 hours in order to form a smooth boride layer through diffusion [2, 26, 28-29].

#### 2.2.2.2 Boriding Agents

Various types of powders, from amorphous pure boron powder to proprietary boron-rich powders have been used to perform boronizing of nickel-based alloys (Table 2.2). BorTec GmbH & Co .KG is a German supplier for various grades of boriding powders with brand name Ekabor®. Some versions of these products are Ekabor® II, Ekabor® III [28] and Ekabor® Ni [30]. Ekabor® II contains 5% $B_4C$, 5% $KBF_4$ and 90% SiC. $KBF_4$ is the activator and silicon carbide (SiC) serves as the diluent. Formation of the boride layer is based on the mechanism that was already described in Fig. 2.5 that is $BF_3$ gas formation which transfers boron atoms on the surface of the substrate to form boride islands [7, 31]. Furthermore, diluent SiC enforces some more reactions to the system by making silicide compounds that assist controlling the rate of layer formation [6, 32]. In other words, when temperature exceeds 600 $^{o}$C, SiC particles oxidize to form a barrier $SiO_2$ on the surface. then, $KBF_4$ decomposes to $BF_3$. Subsequently, reaction between $BF_3$ and $SiO_2$ result in gaseous $SiF_4$ (Eq. 2.1). Therefore, the protective layer of $SiO_2$ is removed partly which

enable further oxidation of SiC. $SiF_4$ tends to react with atoms of nickel and those of other elements to form $Ni_2Si$, $Fe_2Si$, $Ni_5Si$ etc. (Eq.2.2 and 2.3) [6]. The silicide compounds slow the process of boride diffusion and thus limit the thickness of boride layer [6, 33].

**Table 2.2: Chronological sequence of studies on boronizing of nickel-based alloys.**

| Year | Substrate | Method, (Temp. °C), {Time, h} | Thickness (μm) | Composition | Reference |
|---|---|---|---|---|---|
| **1987** | Ni | Pack Boriding, (950), {3} | 40 | $Ni_2B$, $Ni_3B$ | [34] |
| **1987** | Inconel® 600 | Pack Boriding, (950), {3} | 125 | $Ni_2B$, $Ni_3B$ | [34] |
| **1987** | Inconel® 625 | Pack Boriding, (950), {3} | 100 | $Ni_2B$, $Ni_3B$ | [34] |
| **1987** | Inconel® 713C | Pack Boriding, (950), {3} | 50 | $Ni_2B$, $Ni_3B$ | [34] |
| **1987** | Udimet 500 | Pack Boriding, (950), {3} | 40 | $Ni_2B$, $Ni_3B$ | [34] |
| **1987** | Hastelloy B | Pack Boriding, (950), {3} | 60 | $Ni_2B$, $Ni_3B$ | [34] |
| **1999** | Nickel | Pack Boriding, Ekabor® II, (700-900), {10} | 45-100 | $Ni_2B$, $Ni_3B$ | [15] |
| **2000** | Ni | Pack Boriding, Ekabor® II, (950), {2-8} | 123-281 | Exterior: $Ni_5Si_2$, Interior: $Ni_2B$ | [33] |
| **2009** | Pure Nickel | Powder pack | 36-237 | $Ni_2Si$, $Ni_5Si_2$, $Ni_2B$, $Ni_3B$ | [2] |
| **2009** | Ni and Ti | Pack Boriding (950), {1-8 } | 25-140 | $Ni_3B$, $Ni_2B$ | [35] |
| **2013** | Incoloy® 825 | Pack Boriding, Ekabor® II, (900, 950), {2, 4, 6} | 35-170 | FeB, $Fe_2B$, CrB, NiB | [26] |
| **2013** | Inconel® 600 | Electroplating | 80 | $Ni_3B$, $Ni_2B$, NiB, $Ni_4B_3$ | [17] |
| **2013** | Inconel® 718 | Pack Boriding, Ekabor® Ni, (900), {2, 4, 8, 12} | 40 | $Ni_2Si$, $Ni_4B_3$, FeB | [6] |
| **2015** | Inconel® 600 | Gas Boriding (920), {2} | 112 | $Ni_2B$, $Ni_3B$, $Ni_4B_3$, NiB, CrB, $Cr_2B$, Ni | [25] |
| **2015** | Nimonic 80A | Gas Boriding (920), {2} | 105 | $Ni_2B$, $Ni_3B$, $Ni_4B_3$, NiB, CrB, $Cr_2B$, Ni | [25] |
| **2015** | Inconel® 718 | Paste Boriding, (980), {10} | 105-314 | $Ni_2Si$, $Ni_2B$, $Ni_4B_3$, CrB, $Fe_2B$ | [36] |
| **2013** | Inconel® 600 | Laser Boriding | 500 | $Ni_2B$, CrB, $Ni_3B$, $Cr_2B$, Ni, $Fe_3B$ | [37] |

$$3SiO_2 + 4BF_3 \rightarrow 3SiF_4 + 2B_2O_3 \quad \textbf{(2.1)}$$

$$2SiF_4 + 5Ni \rightarrow Ni_5Si_2 + 4F_2 \quad \textbf{(2.2)}$$

$$SiF_4 + 2Ni \rightarrow Ni_2Si + 2F_2 \quad \textbf{(2.3)}$$

The nickel silicide, $Ni_5Si_2$, on the surface has equiaxed granular morphology and $Ni_2B$ has needle-shaped structure. In one study the resulted coating consisted in 281 µm silicide layer on top and only 10 µm boride layer [33].

Due to considerable amount of silicon, Ekabor® II ends up with an inner boride layer and an outer porous silicide layer [2, 37]. While a multi-layer coating has some protective benefits at high temperatures the outer silicide layer is softer than the boride layer and is thus not desirable. Besides, the silicide layer has a very low thermal expansion coefficient compared to the boride layer and thus, if the silicide layer is thick, large residual strain accumulates in the layer leading to crack formation [6-7].

Recently the BorTec GmbH & Co .KG has introduced a new nickel boriding powder formulation, Ekabor® Ni that has less silicon compound agent and thus limits the extent to which a nickel silicide layer forms during boriding [2, 15]. It is this boriding agent that will be used in the studies of this thesis.

### 2.2.2.3 Structure and Composition of a Boride Coating on a Nickel Alloy

The nickel-boron binary phase diagram is shown in Fig. 2.6 and indicates the presence of various $Ni_xB_y$ intermetallic phases [38]. The pack boronizing process naturally results in the development of a boron concentration gradient within the near surface of the boronized nickel alloy [39]. Therefore, NiB, $Ni_4B_3$, and $Ni_2B$, precipitates may exist in different regions of the boron diffusion zone. The final composition of the boride layer (e.g. NiB, $Ni_2B$, $Ni_3B$, $NiB_2$, etc.) depends on the thermodynamic activity of each of the compounds [16]. Table 2.3 shows crystallographic data of the nickel boride phases that are present in a borided nickel-chromium alloy system similar to Inconel® 718 [17].

The morphology of this multiphase boride layer affects many properties of the layer since the hardness of each phase is different ($H_{NiB}$= 1800 $K_{noop}$, $H_{Ni_2B}$ =1400 $K_{noop}$) [11].

Besides, siliciding causes the layers close to the surface be enriched of silicon with $Ni_2Si$ crystals which has low hardness [36]. The resulting coating consists of a top silicate layer or compound layer, a dispersed layer or boride layer consisting of complex nickel/boron

intermetallic compounds and diffusion zone consisting of grain boundary diffusion zone (Fig. 2.7) [6, 18, 34].

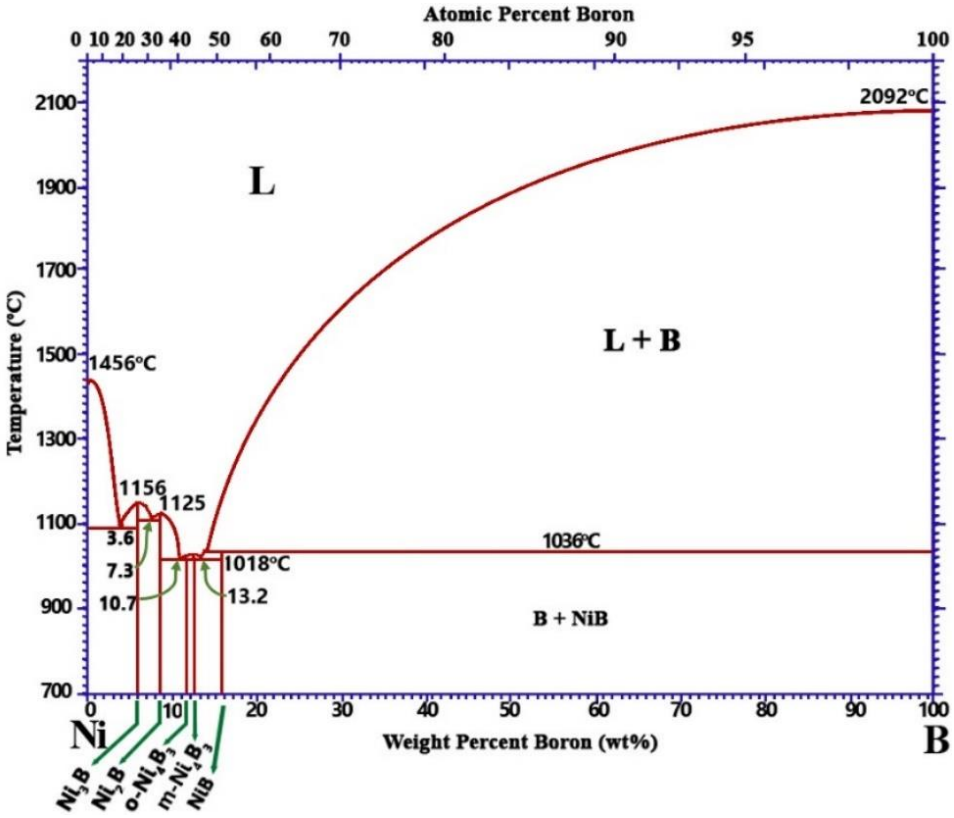


**Figure 2.6: Nickel-Boron binary phase diagram (adapted from [38]).**

**Table 2.3: Crystallographic parameters and coefficient of expansion of nickel and chromium borides [17, 25].**

| **Phase** | **Ni** #70-1849 | **$Ni_2B$** #82-1697 | **$Ni_3B$** #89-3822 | **$Ni_4B_3$** #73-1793 | **NiB** #74-1207 | **$Cr_2B$** #89-4876 | **CrB** #89-3587 |
|---|---|---|---|---|---|---|---|
| **Crystal Structure** | Cubic | Tetragonal | Orthorhombic | Orthorhombic | Orthorhombic | Tetragonal | Orthorhombic |
| **Space Group** | $Fe\bar{3}m$ | 14/mcm | Pbnm | Pnma | Cmcm | 14/mcm | Cmcm |
| **Volume ($Å^3$)** | 43.80 | 105.82 | 151.38 | 234.10 | 64.16 | - | - |
| **Lattice Parameters (Å)** | a = 3.525<br>b = 3.525<br>c = 3.525 | a = 4.992<br>b = 4.992<br>c = 4.2465 | a = 4.389<br>b = 5.211<br>c = 6.619 | a = 11.954<br>b = 2.9815<br>c = 6.5684 | a = 2.925<br>b = 7.396<br>c = 2.966 | a = 5.1850<br>b = 5.1850<br>c = 4.3160 | a = 2.9782<br>b = 7.8790<br>c = 2.9346 |
| **Density ($g/cm^3$)** | 8.90 | 8.05 | 8.20 | 7.58 | 7.20 | - | 6.17 |
| **2θ ($I_{100, \%}$) (Deg.)** | 44.481 | 45.886 | 46.004 | 43.676 | 45.195 | 45.195 | 45.195 |
| **d ($I_{100, \%}$) (Å)** | 2.0352 | 1.9761 | 1.9713 | 2.0708 | 2.0047 | 2.0047 | 2.0047 |
| **Coefficient of Expansion ($°C^{-1}$)** | $11.4 \times 10^{-6}$ | $7.64 \times 10^{-6}$ | $7.9 \times 10^{-6}$ | - | - | - | - |
| #JCPDS Card Number | | | | | | | |

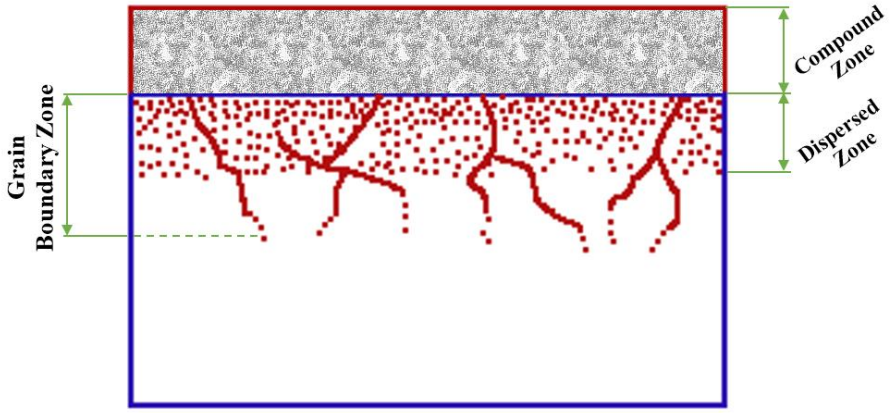


**Figure 2.7: Coating structure of a borided surface (adapted from [34]).**

### 2.2.2.4 Effect of Alloying Elements on Boride Hardness and Thickness

F. Matsuda *et al.* carried out an investigation on the effect of alloying elements on the hardness and thickness of boride coatings. Binary alloys of nickel with either Ti, Zr, Hf, V, Nb, Ta, Cr, Mo, Mn, Fe, Co, Al or Si were prepared and then boronized at 950 $^{o}$C for three hours. The average hardness and thickness of the resulting boride layer is shown as a function of alloy content in Fig. 2.8 [34].

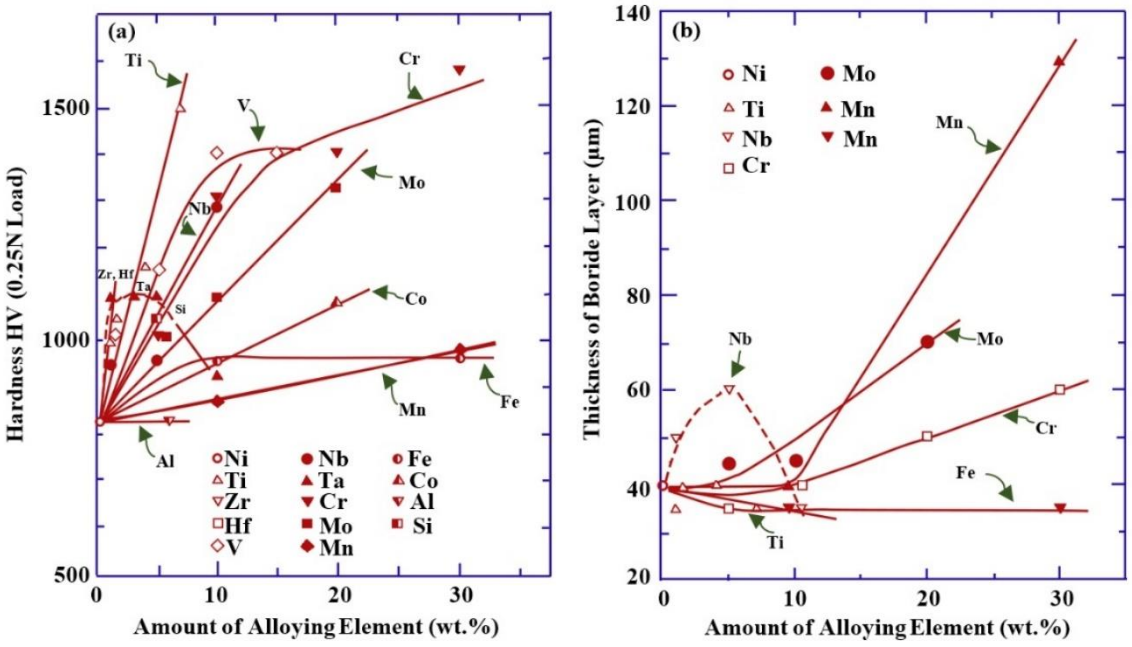


**Figure 2.8: Effect of alloying element on the hardness (a), and coating thickness (b) of a boride layer on a nickel alloy substrate (adapted from [34]).**

Most of alloying elements increase the hardness of the coating layer by forming various types of boride precipitates which are actually harder than the nickel boride phase. Therefore, up to 18% chromium, which is about the same amount as Inconel® 718, significantly increases the hardness of the boride layer. In contrast, Makuch *et al.* reported that alloying elements, such as chromium, often decrease the thickness of the boride layer by increasing the activation energy for solid-state diffusion of boron in nickel [25].

Based on these results Matsuda *et al.* deduced that the most effective alloying elements for improved boride layer hardness and thickness for nickel-based alloys are Ti, Nb (<5 wt.%), V, Cr (>10 wt.%) and Mo [34]. They proposed the following empirical equation to predict the Vickers Hardness (VH) of the boron layer as a function of the chemical composition of the borided alloy as:

$$HV_{alloy} = 220 \times Hf\ (wt.\%) + 170 \times Zr + 95 \times Ti + 54 \times Ta + 46 \times Nb + 44 \times Si + 38 \times V + 25 \times Mo + 13 \times Co + 5 \times Mn + X_{Cr} + Y_{Fe} + 800 \quad \textbf{(2.4)}$$

where,

$$X_{Cr}: 47 \times Cr\ (Cr \leq 10\%),\ 14 \times Cr + 330\ (Cr > 10\%) \quad \textbf{(2.5)}$$

$$Y_{Fe}: 13 \times Fe\ (Fe \leq 10\%),\ 130\ (Fe > 10\%) \quad \textbf{(2.6)}$$

While the form of this equation has great potential usefulness for those considering to use a pack boriding process to surface harden a nickel-based alloy, its empirical nature results in it being quite inaccurate. The measured Vickers hardness of a selection of commercial alloys (Inconel® 600, Inconel® 625, Inconel® 713C, Udimet 400, and Hastelloy B) were about 250 to 610 HV less than that predicted by Eq. 2.4 [34].

### 2.2.2.5 Effect of Time and Temperature on the Boride Layer Thickness

Generally speaking, the thickness of coating increases with time and temperature [40]. Fig. 2.9 illustrates the nonlinear dependence of boride layer thickness upon boriding

temperature and, for a given temperature, the approximately linear dependence of layer thickness upon boriding time [2, 15].

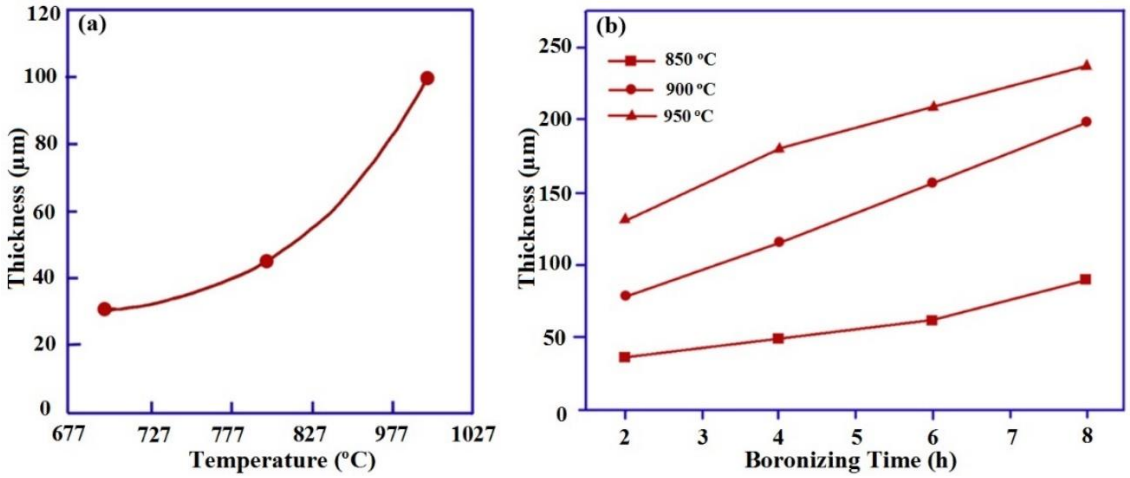


**Figure 2.9: Relationship between (a) boriding temperature, (b) boriding time and boride layer thickness for a nickel-based alloy (adapted from [2, 15]).**

An important observation associated with the study depicted in Fig. 2.9 is that when the boriding process was conducted at a very high temperatures, "flaking of treated layer occurred and thick boride layer was not obtained" [15].

### 2.2.2.6 Wear Properties

As was discussed in section 2.2.2.4, boride compounds significantly improve the hardness of nickel bearing alloys. The wear resistance of nickel-bearing alloys is also improved to the point where borided nickel-based alloys have wear resistance similar to sintered carbides [25]. The amount of metal loss due to wear is about 100 times less for borided samples than for untreated ones [15]. The boride layer can also significantly decrease the coefficient of sliding friction [18]. As a case in point, the coefficient of sliding friction (µ) of untreated Inconel® 718 is about 0.8 while that of borided Inconel® 718 is 0.4 to 0.7 [15, 36]. Higher boronizing temperature causes a harder boride layer with lower coefficient of friction.

# Chapter 3

# 3 EXPERIMENTAL PROCEDURE

In this investigation, the effect of pack boronizing and thermal aging on the indentation hardness and the wear resistance of the nickel-based Inconel® 718 alloy is studied. Samples of this alloy were obtained from VDM METALS Ltd (Nevada, US). The chemical composition of the alloy is shown in Table 3.1 and is within the range defined by SAE AMS 5663M and ASTM A1014-03 [3-4]. The as-received alloy was in the solution annealed condition (982 $^{o}$C for 1 hour followed by water quenching).

**Table 3.1: Chemical composition of Inconel® 718 in comparison with the standard composition range for this alloy [3].**

| Element (wt. %) | Ni | Cr | Nb | Mo | Ti | Co | Al | Mn | Si | Cu | C |
|---|---|---|---|---|---|---|---|---|---|---|---|
| ***Min.*** | 50 | 17.0 | 4.75 | 2.80 | 0.65 | 0 | 0.20 | 0 | 0 | 0 | 0 |
| ***Max.*** | 55 | 21.0 | 5.50 | 3.30 | 1.15 | 1 | 0.80 | 0.35 | 0.35 | 0.3 | 0.08 |
| **Sample** | 53.96 | 18.34 | 5.33 | 3.03 | 0.96 | 0.20 | 0.61 | 0.08 | 0.06 | 0.05 | 0.030 |
| **Element (wt. %)** | **Ta** | **Ca** | **S** | **P** | **B** | **Mg** | **Pb** | **Se** | **Bi** | **Fe** | |
| ***Min.*** | 0 | - | 0 | 0 | 0 | - | 0 | 0 | 0 | Bal. | |
| ***Max.*** | 0.05 | - | 0.015 | 0.015 | 0.006 | - | 0.0005 | 0.0003 | 0.00003 | | |
| **Sample** | 0.01 | <0.010 | 0.001 | 0.008 | 0.004 | 0.0030 | 0.0001 | <0.0001 | 0.00001 | 17.22 | |

Two sets of samples were prepared from the Inconel® 718 material (Fig. 3.1): i) The first set were cylindrical buttons of 10 mm diameter and 6 mm height. These samples were used for microstructural studies and hardness measurements. ii) The second set was cylindrical discs and pins used for wear evaluations. The cylindrical discs were of 6.4 mm thickness with 6.4 and 25.4 mm inner and outer diameter respectively. The pins were of 6.4 mm diameter and 25.4 mm length. Two samples were made of each set for each thermal condition described in Section 3.1. Both flat surfaces of the samples were then prepared by mechanical grinding with successively finer, from 800 to 2000 grit, SiC abrasive paper followed by polishing with 1 µm diamond paste.

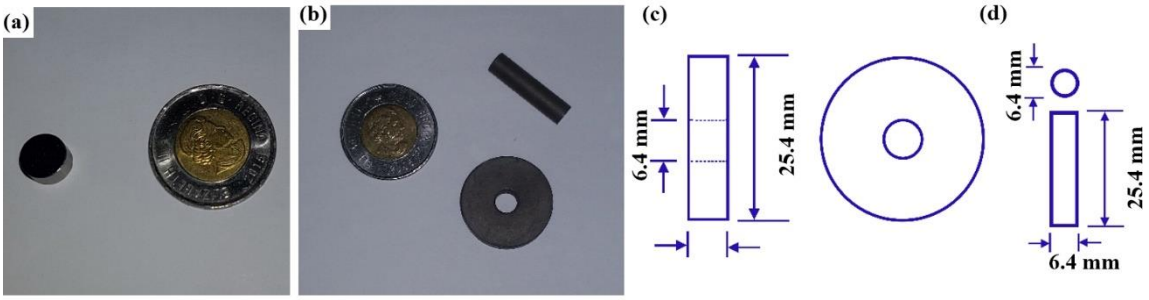


**Figure 3.1: Inconel® 718 samples (a) button sample; (b) disc and pin wear test sample; (c) disc dimensions; (d) pin dimensions.**

## 3.1 Thermal Treatments

The polished Inconel® 718 samples were then subjected to two thermal processes i) age hardening (aging) and/or ii) pack boronizing. The order of the processes was changed to investigate the effect of the combined processes on the overall hardness and wear resistance of the alloy. The following five conditions were considered:

- **AB**: In this condition the samples were first aged and then boronized.
- **BA**: In this condition the samples were first boronized and then aged.
- **SAB**: In this condition the samples were simultaneously aged and boronized.
- **JB**: In this condition the samples were just boronized and not aged.
- **JA**: In this condition the samples were just aged and not boronized.

For simplicity, these conditions will be referred to by their abbreviations. The Aging and Boronizing thermal treatments are described below.

### 3.1.1 Aging Treatment

Aging thermal treatment was performed according to ASTM A1014-03 and ASTM B 637-12 [3, 9]. The samples were heated in vacuum ($6.6 \times 10^{-2}$ torr) up to 718 °C for 8 hours, followed by slow cooling (100 °C/hr) to 620 °C, held at this temperature for another 8 hours, and cooled in air to room temperature. The aging thermal treatments were performed in an Ipsen vacuum induction furnace located at Surface Heat Treat and Coating Co. in Hamilton, Ontario (Fig. 3.2).

**Figure 3.2: Vacuum furnace employed for aging treatment.**

### 3.1.2 Boriding Treatment

Boronizing was performed in a Thermo-Thermolyne FD 1500 Industrial Furnace (Fig. 3.3) operating with a flowing Ar gas atmosphere to prevent oxidation of the samples. This furnace is located at Surface Heat Treat and Coating Co. in Hamilton, Ontario. The boriding agent used in this project was Ekabor® Ni powder purchased from BorTec Co. of Germany. The exact chemical composition of the Ekabor® Ni powder is proprietary and, hence not available, however previous researchers have analysed its composition with X-ray diffraction analysis and have reported that it contains little or no SiC but contains $Ca_6B$ and traces of $KBF_4$ activating powders [2]. The Inconel® 718 samples were placed in small steel containers which were then packed with the Ekabor® Ni powder.

For the AB, BA, and JB samples, the packed containers were heated to the boriding temperature of 800 $^oC$ and held for 5 hours. For the SAB samples the boriding was done in same furnace but with a thermal cycle that would promote concurrent age hardening of the Inconel® 718 samples (718 °C for 8 hours, cooling down with rate 100 °C/hr and holding at 620 °C for 8 hours (Fig. 3.4)).


**Figure 3.3: Thermo-Thermolyne FD 1500 industrial furnace.**

## 3.2 Evaluations and Equipment

After the aging and/or boronizing thermal treatments, the surface morphology/roughness, microstructure, indentation hardness, and wear resistance of the Inconel® 718 samples were evaluated using the equipment and methodologies described below.

### 3.2.1 Surface Morphology and Roughness Measurements.

The surface morphology of the aged and borided samples was studied by optical and scanning electron microscopy (SEM). The optical microscope used was a Nikon Eclipse L150 equipped with Nikon Digital Eclipse DXM1200 camera (Fig. 3.5 (a)) while the SEM was a JEOL JXA-8530F field-emission analytical scanning electron microscope equipped with secondary- and back scattered-electron detectors and a wavelength dispersive (WDS) X-ray detector capable of semi-quantitative chemical analyses (Fig. 3.5 (b)).

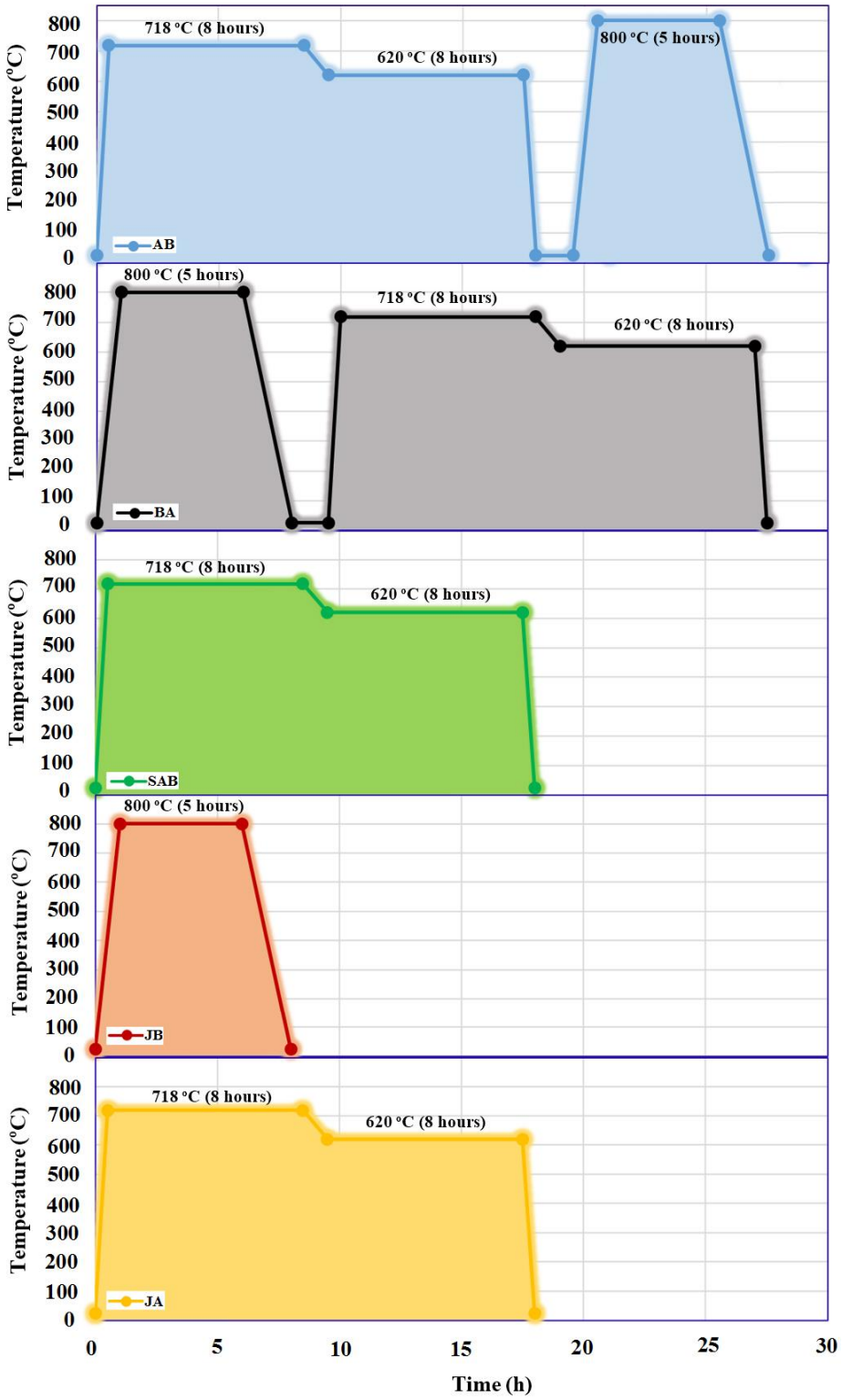


**Figure 3.4: Temperature-Time histories of samples subjected to the AB, BA, SAB, JB, and JA thermal treatments.**

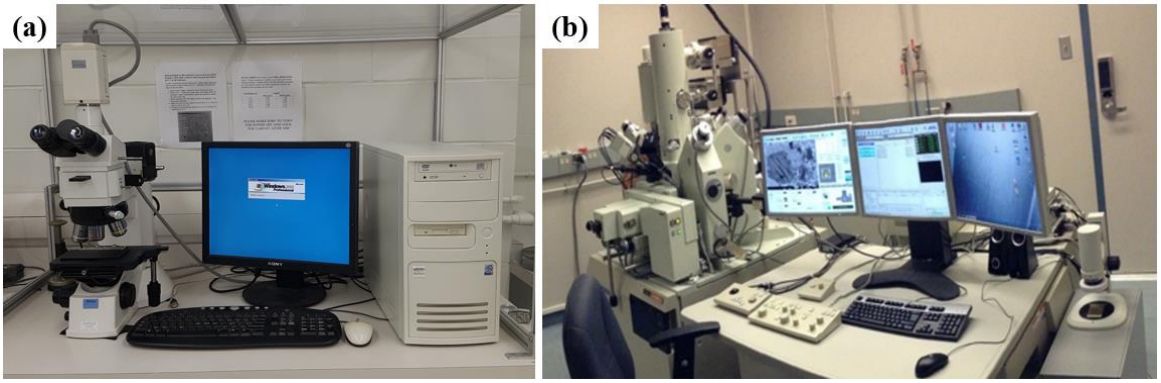


**Figure 3.5: (a) Nikon Eclipse L150 optic microscope; (b) SEM microscope (JEOL JXA 8530F).**

The surface roughness of the samples was measured with a Micro Materials Nano Test indention machine (Fig. 3.6 (a)). This machine consists of a ceramic pendulum on top of which an electric coil is mounted (Fig. 3.6 (b)). Passage of an electric current through the coil induces a magnetic field causing the pendulum to be attracted to the magnet. As a result, the pendulum swings around the pivot, located at its midpoint, causing the sharp conical diamond indenter, attached to the lower side of the pendulum, to swing toward and lightly contact the surface of the sample. By maintaining a fixed electrical current to the coil, a small constant indentation force is applied to the sample. A parallel plate capacitor, located between the bottom of the pendulum and the fixed base of the instrument, is used to measure, with high precision, the change in position of the indenter as the sample is moved by computer-controlled micrometers, on an Y-Z plane perpendicular to the indenter.

The surface roughness of the samples of this study were measured, with this instrument, using a conical indenter with a 5 μm diameter tip under the application of a small 0.1 mN indentation load. The samples were moved along the Y- and Z-axes (The indentation direction was along the orthogonal X-axis) a distance of 200 ± 5 μm while the displacement of the indenter, indicating the surface roughness, was continuously recorded. Five parallel horizontal (Y-axis) and five parallel vertical (Z-axis) scans, each spaced 20 μm apart, were performed on samples from each of the five thermal conditions. An example of a typical surface roughness measurement is depicted in Fig. 3.7 (a) and (b). The straight black lines show the path of scanning while the blue lines illustrate the X-axis height deviation of the indenter from its mean height as determined by the Nano Test indentation software.

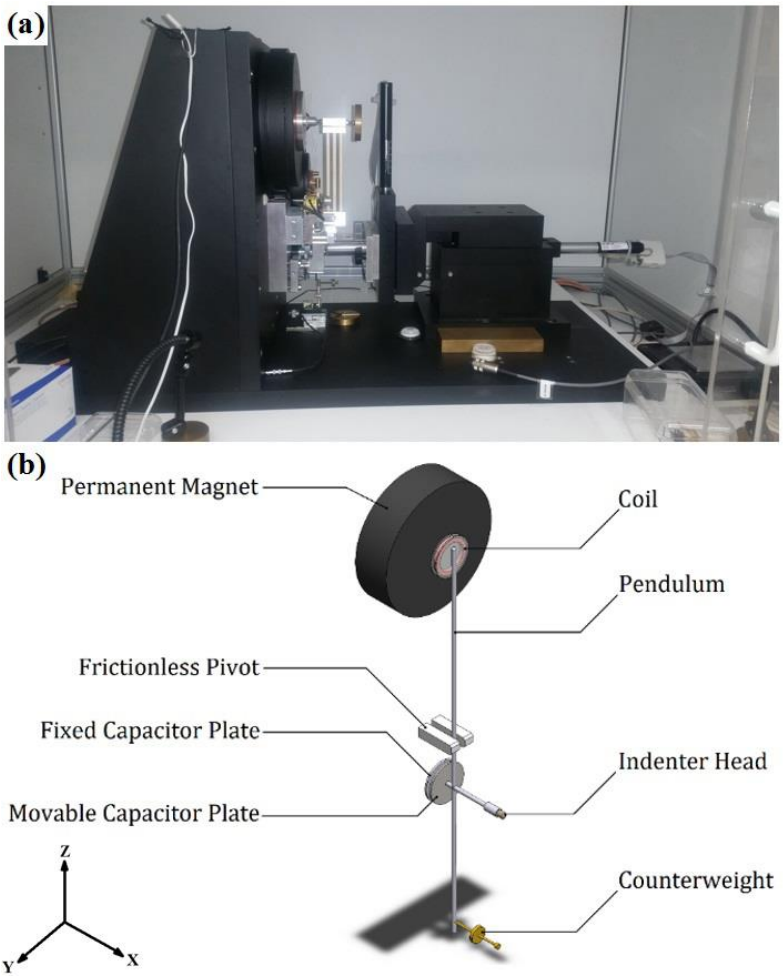


**Figure 3.6: (a) The Micro Materials Nano Test Indentation testing machine; (b) load applying and displacement measurement system (adapted from [41]).**

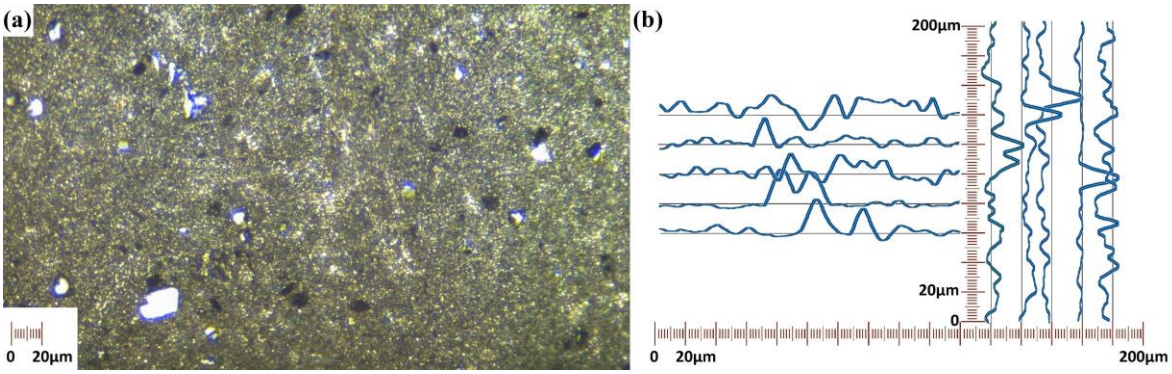


**Figure 3.7: (a) Roughness condition of sample AB and (b) typical surface roughness measurements.**

The acquired X-axis height data were used to calculate the average root mean square of asperity height ($R_{rms}$) characteristic of the surface roughness of each sample as

$$R_{rms} = \sqrt{\frac{1}{n}\sum_{i=1}^{n} x^2} \quad \textbf{(3.1)}$$

where $x$ is vertical distance from the mean of the surface at the $i^{th}$ measurement point and $n$ is the total number of measurement points in the scan.

### 3.2.2 Microstructural Phase Analyses

The microstructural phases present in the surface region of the aged and/or borided Inconel® 718 samples were analyzed by X-ray diffraction using a Bruker D8 Advance diffractometer (Fig. 3.8). A Cu Kα X-ray source (λ = 15.406 Å) was directed on the surface of the sample and scanned over a range of angles θ relative to the surface normal direction from 2θ = 10 to 90 degrees. The X-ray diffraction signal was obtained as a function of θ and the angular position of the Bragg reflection peaks was used to identify the crystal phases present in the material. This identification was done using the X'Pert HighScore software manufactured by PANalytical B.V.

### 3.2.3 Further Microstructural Characterization

Several samples from each thermal condition (AB, BA, SAB, JA, and JB) were electroplated with a pure copper layer on the borided surface to protect the surface from rounding during subsequent grinding and polishing operations. The electroplating was done in an aqueous copper sulfate ($CuSO_4$) solution electrolyte. A pure copper plate was used as the anode and the sample to be protected was the cathode. A current density of 4 A/dm$^2$ was used for 24 hours to deposit a coating layer of more than 100 µm thickness onto the sample surface.

The copper plated samples were then sectioned, perpendicular to the borided surface, with a Buehler IsoMet® low speed diamond saw. The sectioned samples were then mounted in 35 mm diameter disks of fast cure epoxy. The cut surface, perpendicular to the borided surface, was then ground with successively finer grades of SiC paper from

800 to 4000 grit. The ground surfaces were then polished with a Buehler Inc. Mastermet 2 colloidal silica, 20 nm diameter, aqueous suspension.

To reveal and compare grain size and shape in the regions near the borided surface the sectioned Inconel® 718 samples were etched with Marble's reagent (10 ml nitric acid ($HNO_3$), 10 ml acetic acid ($CH_3COOH$), 15 ml hydrochloric acid (HCl) and 5 drops glycerine) according to the procedure described in ASTM E 407 [42]. Etching was done by immersion of the sample in the etchant for between 5 to 7 seconds. This process revealed the grain structure clearly and allowed the thickness of the borided layer as well as the grain size to be measured using the established procedure described in ASTM E 112-13 [43].


**Figure 3.8: Bruker XRD D8 Advance used for composition studies of the coating.**

## 3.2.4 Indentation Hardness Tests

### 3.2.4.1 Nanoindentation Hardness Measurements

In order to understand the local variation in hardness resulting from surface coating or hardening operations it is necessary to perform nano- rather than micro-indention hardness tests. In this study we used a Micro Materials Nano Test indentation machine (Fig. 3.6) to perform these nanoindentation hardness measurements. The tests were performed using a three-sided pyramidal diamond indenter with 50 nm tip radius.

For these tests the indentation force ($F$) was applied at a constant loading rate of 0.1 mN/s to a maximum indentation depth of $h_{max}$ = 300 nm. The nanoindentation tests were performed on the sectioned Inconel® 718 samples (Section 3.2.2). Multiple nanoindentations were performed on the plane along a line that began within the bulk sample, over 25 μm away from the borided surface and extended to, and across the borided layer by every 1 μm steps. The nanoindentations were spaced about 30 μm apart along the line to avoid the interaction of one on another (Fig. 3.9). Each indentation test was repeated up to 9 times. The nano indentation hardness was determined from the $F$ versus $h$ data (Fig. 3.10) obtained from each indentation test using established methods [44-45].

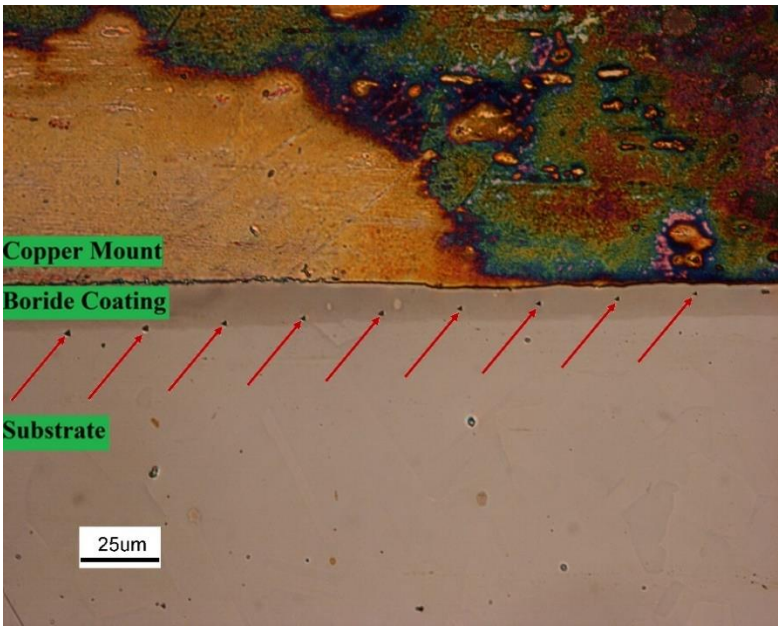


**Figure 3.9: Optical image of a typical line of indentations extending from the bulk sample across the borided region in SAB sample.**

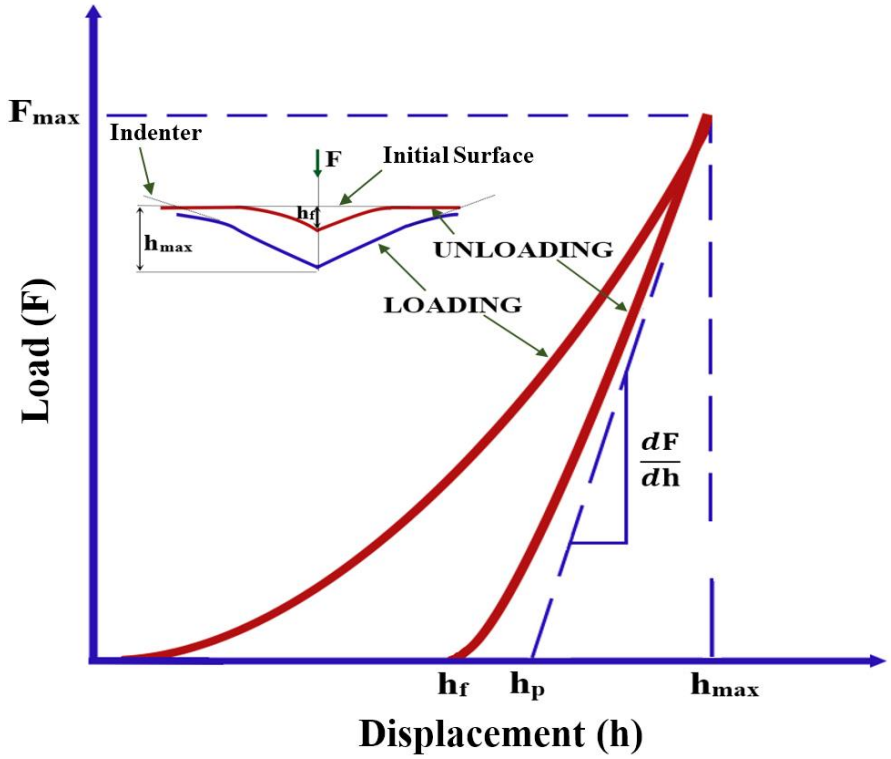


**Figure 3.10: Loading-unloading *F* - *h* diagram obtained from a typical nano indentation test (adapted from [44, 45]).**

The projected area ($A_p$) of the indentation is related to the plastic indentation depth ($h_p$), as:

$$A_p = 24.5\ h_p^2\ [\text{mm}^2] \qquad \textbf{(3.2)}$$

This equation is valid when the tip of indenter is ideally sharp. However, the original Berkovich indenter has a tip with 50 nm in radius while the indenter becomes blunter during service. To avoid error in hardness measurements, "diamond area function calibration'' was periodically performed. It is calculating the hardness of a standard sample (fused silica) with known hardness (9-10 GPa) at various indentation depths. From these data the projected contact area ($A_p$) can be determined at each indentation depth ($h_p$). A high order polynomial function is then fitted to the data to express $A_p(h_p)$:

$$A_p(h_p)=A_1h^5+ A_2h^4+ A_3h^3+ A_4h^2+ A_5h+ A_6 \qquad \textbf{(3.3)}$$

This polynomial contact area function is then used to calculate the indentation hardness of the test samples as:

$$H = \frac{F}{A_p(h_p)} \quad \textbf{(3.4)}$$

### 3.2.4.2 Microindentation Hardness Measurements

Vickers microindentation hardness measurements were performed on samples from each thermal condition (AB, BA, SAB, JA, and JB) to assess the hardness of i) the boride coatings, ii) the transition region below the borided layer, and iii) the bulk material. The microindentation tests impose a relatively "large" indentation, of several tens of micrometers dimension, into the material and thus the hardness value obtained from these tests represents the average hardness of the material. The Vickers microhardness number (VHN) is an industrial standard for characterizing the yield strength of common engineering metals since VHN $\approx 3\sigma_{yield}$ [46]. In this study microindentation hardness tests were performed, according to established procedure as described in ASTM E 384 [47], with a Buehler Micromet II Vickers microhardness tester (Fig. 3.11).


**Figure 3.11: Buehler Micromet II micro hardness tester.**

For each sample, 5 to 7 indentations were made in each of the three regions described above at indentation forces of $F$ = 0.01, 0.025 and 0.05 kgf. The diagonal length ($d$) of the resulting diamond shaped indentations was measured optically and the Vickers indentation hardness number was calculated as:

$$HV = \frac{F}{A} \approx \frac{1.8544F}{d^2} \text{ [kgf/mm}^2\text{]} \quad \textbf{(3.5)}$$

### 3.2.5 Wear Behavior

A wear machine was developed for this project based on the published standards for pin-on-disc wear testing, ASTM G 99 (Fig. 3.12 (a)). In this test, two specimens of the same material become in contact, a disc and a pin. The disc is fixed at the center of a horizontally aligned revolving wheel while the pin is perpendicularly in contact at a distance from the central point of the disc. Therefore, a sliding path forms through rotation of the disc. A suspending weight is applied over the pin to intensify the wear condition (Fig. 3.12 (b)).

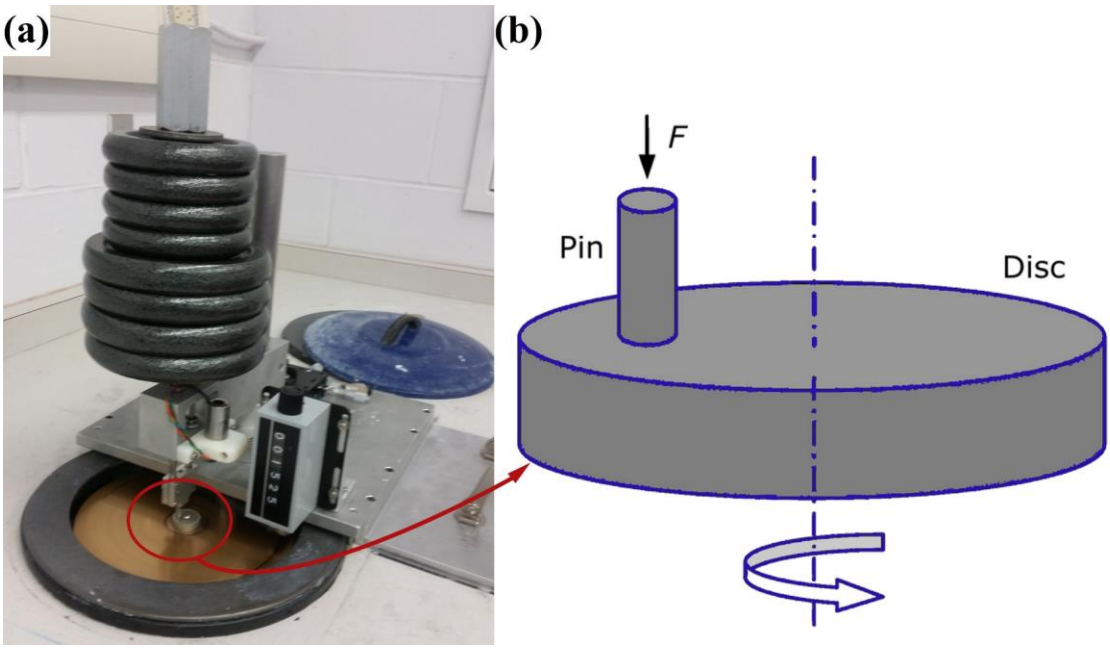


**Figure 3.12: (a) Developed pin on disc wear test machine; (b) Principles of pin on disc test (adapted from [48]).**

The machine is capable of applying a load up to 160 N to an Inconel® 718 pin of 6.4 mm diameter. The loaded pin is then placed in contact, 8 mm from the central axis, of a 25.4 mm diameter flat disc made of the same material. Pin-disc sets from each Inconel® 718 sample conditions (AB, BA, SAB and JA) were constructed and tested with this apparatus.

Before each test, the pin and disc components were degreased in acetone and isopropanol and then weighed with a high precision laboratory scale (± 0.0001 g). Wear tests were performed in the dry, nonlubricated condition under pin-disc contact pressures of 2.5, 3.3, 4.0 and 4.7 MPa. Each wear test was performed to a sliding distance of 1000 m. Each test was intermittently stopped at 100 m sliding distance increments and the pin and disc were ultrasonically cleaned in acetone and isopropanol to remove debris and wear products and then reweighed. The accumulated weight loss of the samples was recorded as a function of contact pressure and sliding distance. At the end of the wear test the wear tracks on the discs were observed both optically and with SEM to understand the nature of wear process.

# Chapter 4

# 4 RESULTS

In this study microstructural analyses, indentation hardness tests, and sliding wear tests were performed on borided and/or age hardened Inconel® 718 alloy samples to determine the most effective way to apply a nickel boride hard surface while still retaining the high mechanical hardness of the age hardened Inconel® 718 alloy. In this chapter, we present the results of the analyses on the samples made under the five conditions:

- **AB**: In this condition the samples were first aged and then boronized.
- **BA**: In this condition the samples were first boronized and then aged.
- **SAB**: In this condition the samples were simultaneously aged and boronized.
- **JB**: In this condition the samples were just boronized and not aged.
- **JA**: In this condition the samples were just aged and not boronized.

## 4.1 Microstructural Analyses

### 4.1.1 Surface Roughness

The data of the typical roughness profiles is shown in Table 4.1. The root mean square of asperities ($R_{rms}$) was calculated using Eq. 3.1. The polished surface of the starting solution annealed (as received (AR)) Inconel® 718 sample has the lowest RMS surface roughness (22 µm). The just aging (JA) process increases the roughness slightly (49 µm) however the boriding process (AB, BA, SAB, or JB) results in substantially increased surface roughness (388 to 857 µm).

**Table 4.1: Root mean square of surface roughness ($R_{rms}$) of the Inconel® 718 samples subjected to various aging/boriding conditions.**

| Sample | AR | JA | AB | SAB | JB | BA |
|---|---|---|---|---|---|---|
| **Root Mean Square of Roughness ($R_{rms}$) (µm)** | 22 | 49 | 675 | 388 | 530 | 857 |

Fig. 4.1 shows optical and scanning electron micrographs of the just aged (JA) Inconel® 718 samples. In contrast, Fig. 4.2, 4.3 and 4.4 depict the rougher surfaces of the borided (JB, AB, SAB, and BA) samples. These figures indicate, for all boriding

conditions, a relatively uniform boride layer was created with only small regions of imperfections as shown by the un-sintered particles labelled in Fig. 4.3. The unsintered or unreacted crystalline structures of Ekabor® Ni particles are obvious in JB, AB and SAB (Fig. 4.3), but not in BA.

### 4.1.2 Structure and Thickness of the Boride Layers

Fig. 4.5 shows optical images of polished sections perpendicular to the borided surface of the Inconel® 718 samples. The boride layer is of generally uniform thickness around the sample for all conditions. The etched surface of the selected sections in Fig. 4.5 is shown in Fig. 4.6. The chemical etching process revealed that the boride layer consists of two zones: i) the Dispersed Zone (DZ) where the nickel boride is present as a continuous phase and ii) the Grain Boundary Zone (GBZ) where significant diffusion of boron, and hence precipitation of nickel boride, occurs only along pre-existing grain boundaries. These two zones are labelled in Fig. 4.6. The thickness of the DZs, GBZs, and overall boride layer are given in Table 4.2 for each boriding condition tested.

A significant observation that can be made from Fig. 4.5 is the tendency of the JB, AB, and SAB samples to contain large cracks running through the DZ region of the boride layer. No crack was observed in the boride layer of the BA samples.

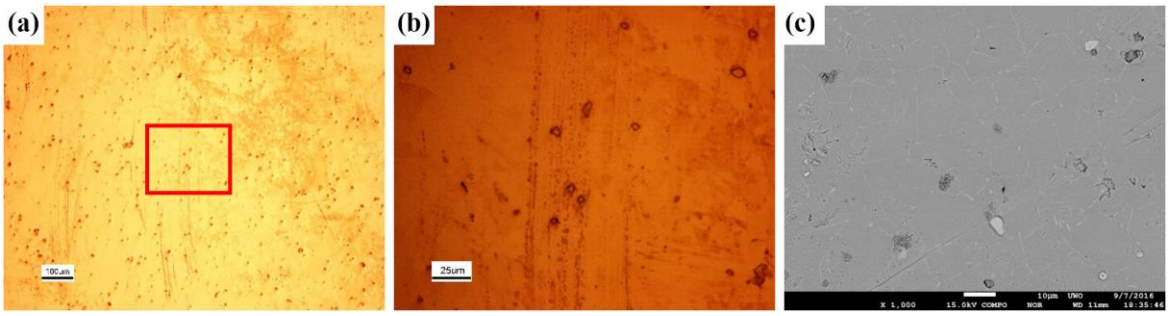


**Figure 4.1: Surface condition in just aged (JA) condition. (a) 100X, (b) 500X and (c) 1000X.**

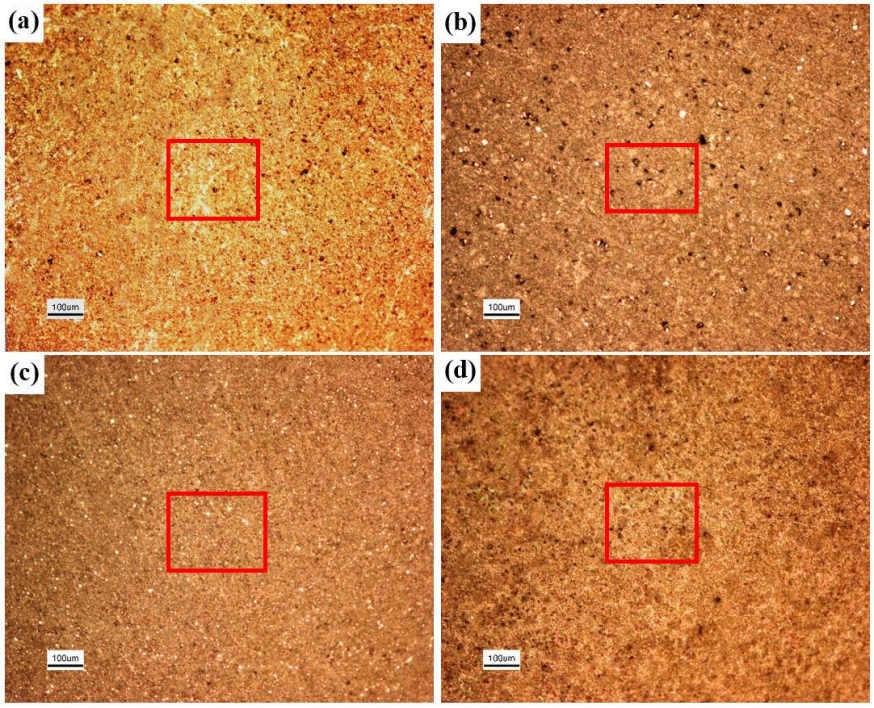


**Figure 4.2: Surface appearance after coating process at 100X; (a) JB, (b) AB, (c) SAB, (d) BA.**

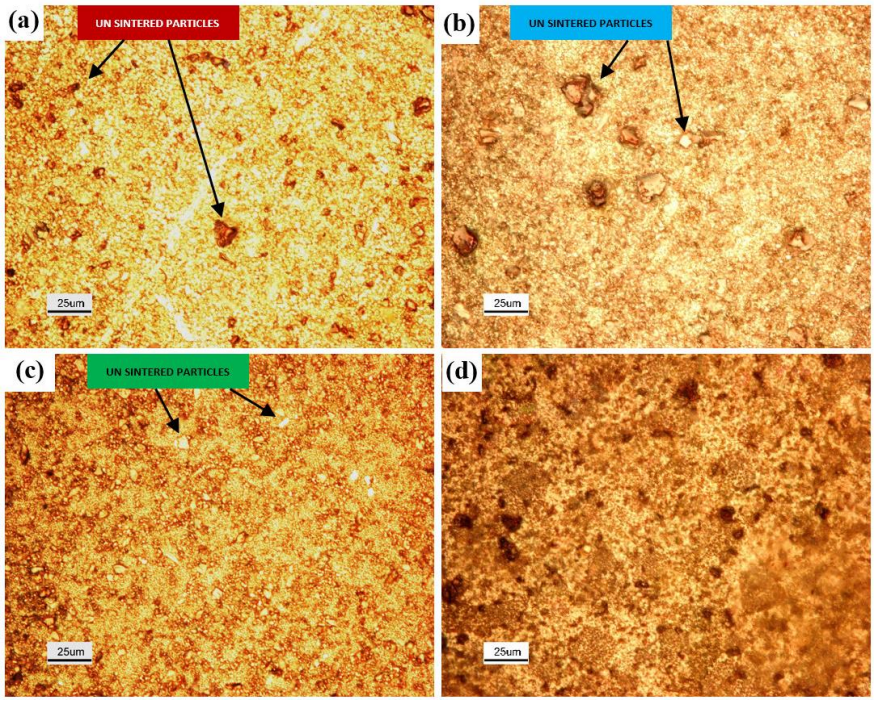


**Figure 4.3: Surface appearance after coating process at 500X. (a) JB, (b) AB, (c) SAB, (d) BA.**

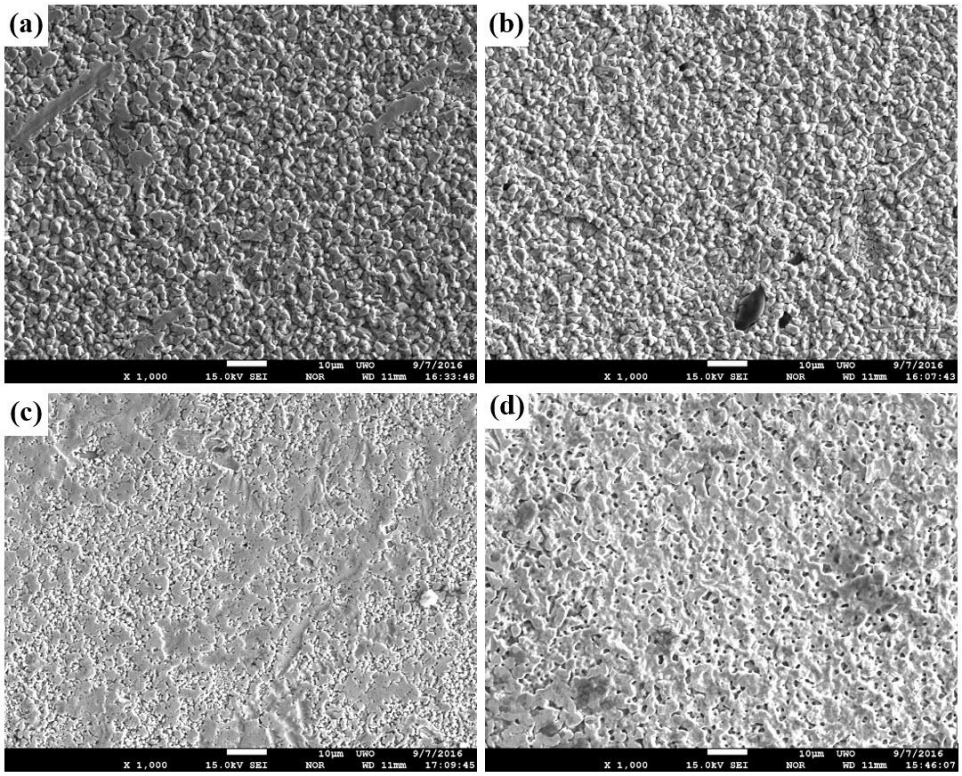


**Figure 4.4: SEM micrographs of coating surface at 1000X; (a) JB, (b) AB, (c) SAB, (d) BA.**

## 4.1.3 Chemical Composition of the Coating

As a precursor to our assessment of the chemical composition and phase identification within the various boride layers, X-ray diffraction analysis was performed on the starting Ekabor® Ni powder that was used as the pack in all the boriding treatments performed in this study. While the exact chemical composition of the Ekabor® Ni powder is classified, previous researchers have analysed its composition with X-ray diffraction analysis and have reported that it contains little or no SiC but contains $Ca_6B$ and traces of $KBF_4$ powders [2]. Fig. 4.7 shows the indexed X-ray diffraction peaks obtained from a backscattered analysis of the Ekabor® Ni powder. The powder is composed of $B_4C$, $Si_6B$, $CaF_2$, and $Ni_2O_3$. This composition is substantially different than what was previously reported [2].

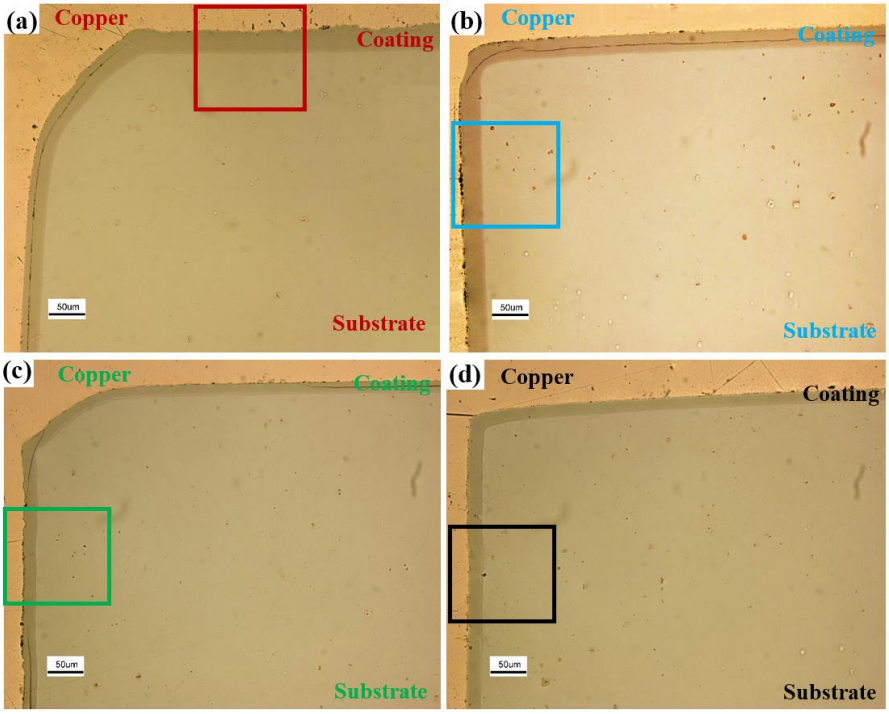


**Figure 4.5: Unetched optical micrographs of the uniform boride layer on samples from the (a) JB, (b) AB, (c) SAB, and (d) BA conditions.**

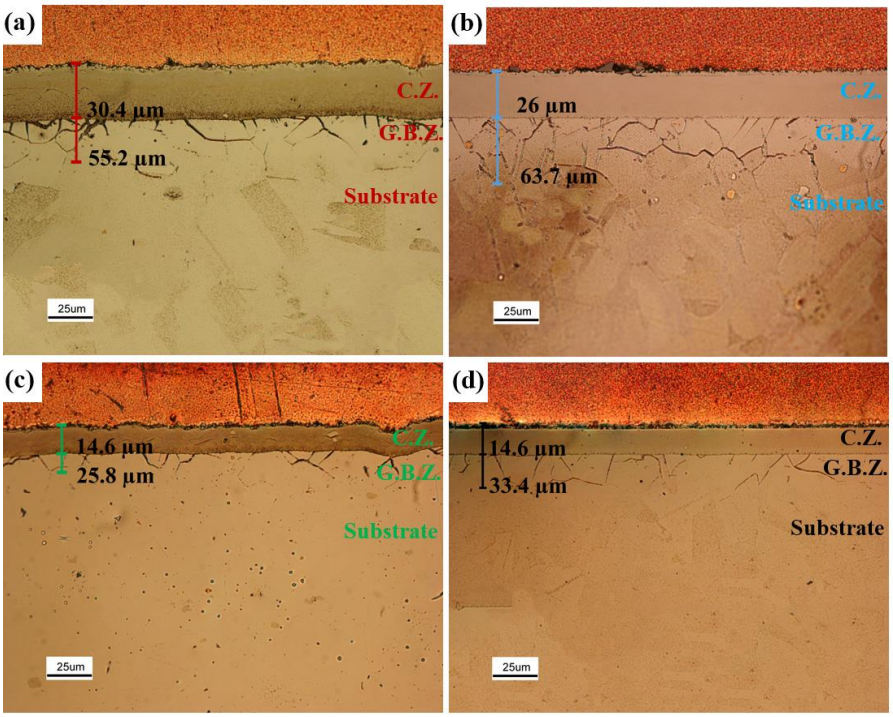


**Figure 4.6: Optical micrographs of the chemically etched boride layer on samples from the (a) JB, (b) AB, (c) SAB, and (d) BA conditions.**

**Table 4.2: Average boride coating thickness for different conditions.**

| Condition / Thickness (µm) | JB | AB | SAB | BA |
|---|---|---|---|---|
| **Dispersed Zone** | 29.5 | 25.6 | 15 | 15.1 |
| **Grain Boundary Zone** | 24.5 | 32.8 | 9.9 | 20.3 |
| **Overall** | 54.0 | 58.4 | 24.9 | 35.4 |

Similar to described mechanism in Fig. 2.5, in this Ekabor® Ni powder mixture, the $B_4C$ and $Si_6B$ act as the boron carrying agent, the $CaF_2$ acts as an activator to encourage the decomposition of the carrying agents and the precipitation of nickel- or iron- borides, while the $Ni_2O_3$ is a filler powder. The presence of silicon in the Ekabor® Ni powder results in the possibility of $Ni_xSi_y$ precipitation during the subsequent boriding process.

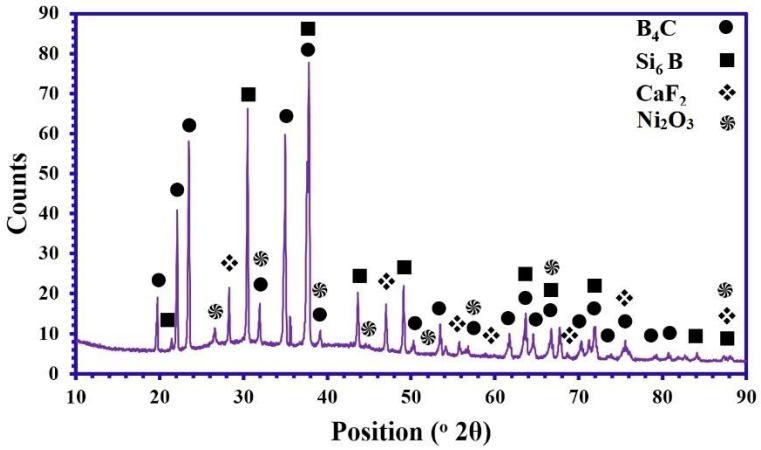


**Figure 4.7: Indexed X-ray diffraction profile of the Ekabor® Ni boriding powder.**

Indexed X-ray diffraction peaks of the borided layers (JB, AB, SAB, and BA) are shown in Fig. 4.8. These profiles indicate that a variety of nickel-/iron-borides, chromium-/molybdenum-borides, nickel-silicides, and nickel-oxides are present in the borided layer of the samples and the phases present are dependent upon the boriding/aging treatment.

Fig. 4.9 shows SEM WDS X-ray boron and silicon composition maps of the polished planes perpendicular to the various borided surfaces. A notable finding shown in these figures is that nickel silicides appear on the top surface of the boride layer under certain boriding conditions (particularly the AB condition).

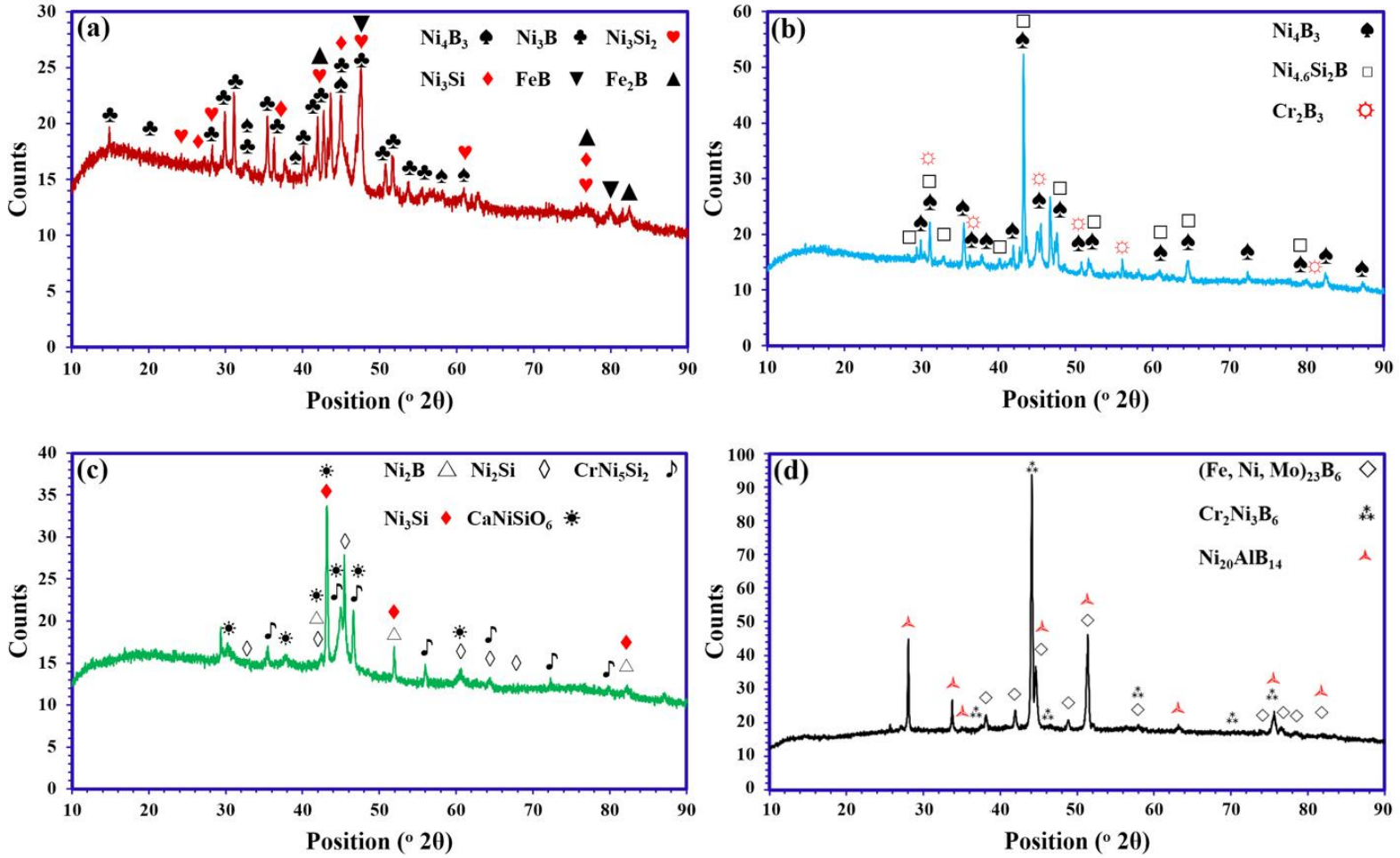


**Figure 4.8: X-ray diffraction profiles of borided surface of samples in various boride conditions: (a) JB; (b) AB; (c) SAB; (d) BA.**

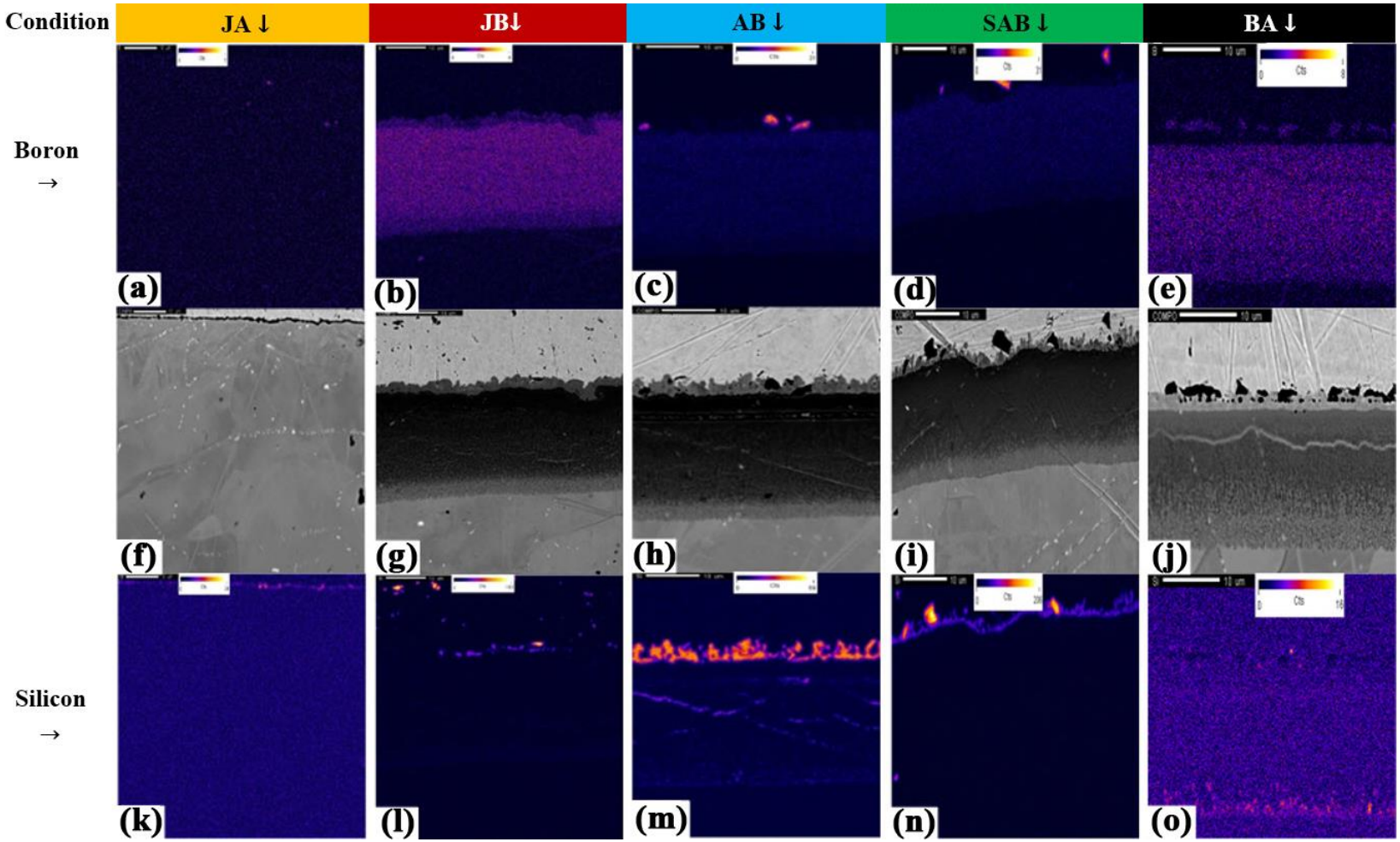


**Figure 4.9: SEM WDS X-ray composition maps of aged and borided Inconel® 718 samples reveal the presence of boron and silicon in the borided layer.**

Fig. 4.10 shows more details of chemical analysis in the boride layer of the AB condition. These observations reveal that the boride layer is actually composed of two sections; i) a thin, 2-4 µm thick, nickel silicide layer at the top (Compound Zone) and ii) a thicker underlying nickel-/iron-/chromium-boride layer (Dispersed Zone). X-ray point analyses indicate that the amount of nickel in the upper region (i) is 80% while it is about 40% in the lower region (ii), and about 52% in substrate Inconel® 718.

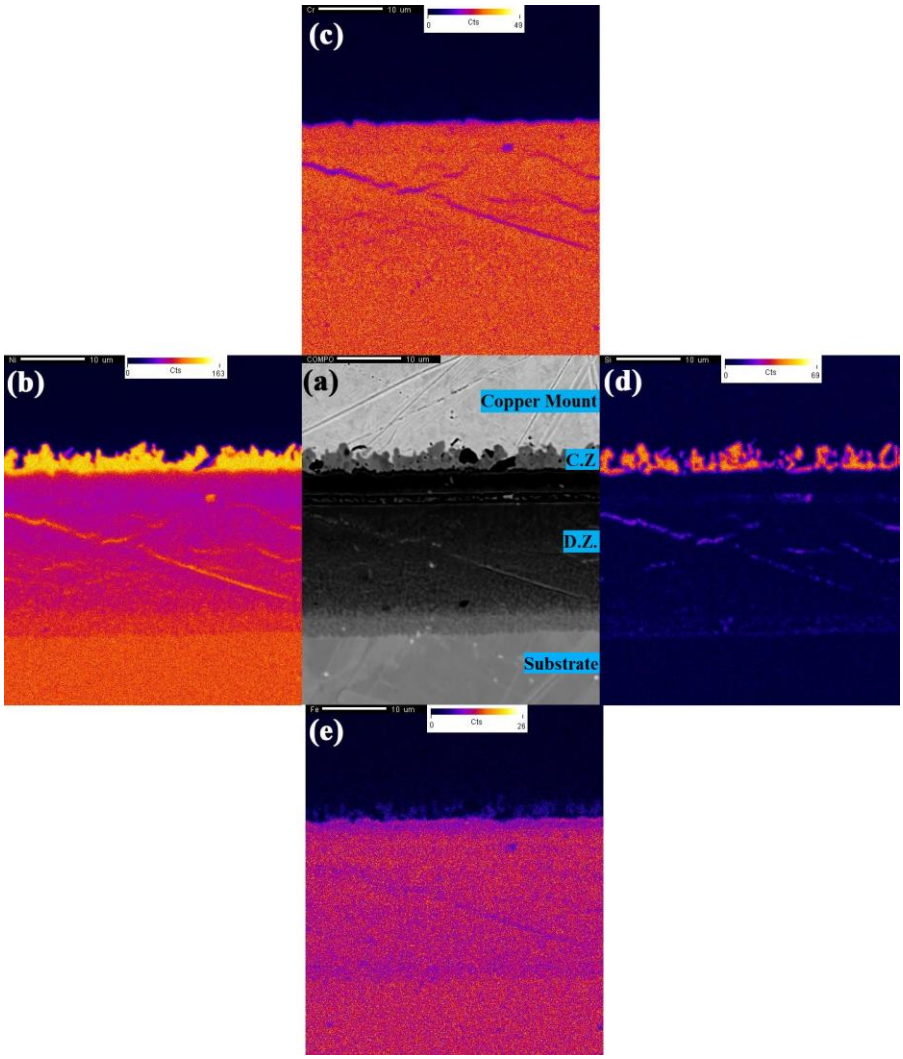


**Figure 4.10: SEM BSE image (a), and WDS map of AB sample for (b) Ni, (c) Cr, (d) Si, (e) Fe.**

Fig. 4.9 indicates that the thickness of the nickel silicide region is very dependent upon the boride/aging condition and, in some cases no nickel silicide region appears despite the fact

that all the samples were produced from the same Ekabor® Ni boride powder. This disparity is discussed in Chapter 5.

## 4.2 Hardness of the Coating

### 4.2.1 Nanoindentation Hardness

Table 4.3 summarizes measured nanoindentation hardness while Fig. 4.11 depicts the indentation track across the coating layer and the corresponding typical measured hardness profile of the various borided/aged Inconel® 718 samples. The nanoindentation tests were performed in parts of the coating that contained cracks in order to assess whether the cracking corresponded to regions in the coating that displayed very high, or very low, local hardness.

**Table 4.3: Nanoindentation hardness test results of the various borided/aged Inconel® 718 samples.**

| Condition | Maximum Hardness (GPa) {HV} | Average Thickness (µm) | Total thickness of hardened layer (µm) | Hardness at Crack (GPa) {HV} | Hardness of the Bulk (GPa) {HV} |
|---|---|---|---|---|---|
| **JA** | - | - | - | - | 8.9 {907.5} |
| **JB** | 31.2 {3181} | 25 | 30 | 21.4 {2182} | 5.7 {581} |
| **AB** | 30.5 {3110} | 29 | 32 | 7.2 {734} | 8.2 {836} |
| **SAB** | 27.2 {2774} | 13 | 16 | 12.9 {1315} | 9.4 {958} |
| **BA** | 25.3 {2580} | 15 | 20 | - | 7.8 {795} |

The Just Aged (JA) sample displayed a uniform hardness with little hardness variations from the edge to the bulk of the sample (average hardness 8.9 GPa). The borided samples, on the other hand, displayed significantly increased hardness in the borided region. The hardness within the borided region of these samples was between 20 to 31 GPa.

Table 4.3 indicates that the Just Borided (JB) samples had the lowest bulk hardness (5.8 GPa) while the aged samples (JA, AB, BA and SAB) displayed the highest bulk hardness (7.5 to 9.4 GPa). The variability in the bulk hardness of the samples that were both borided and aged reflects the effect of the boriding thermal process on the microstructure created during the aging process. This will be discussed in more detail in Chapter 5.

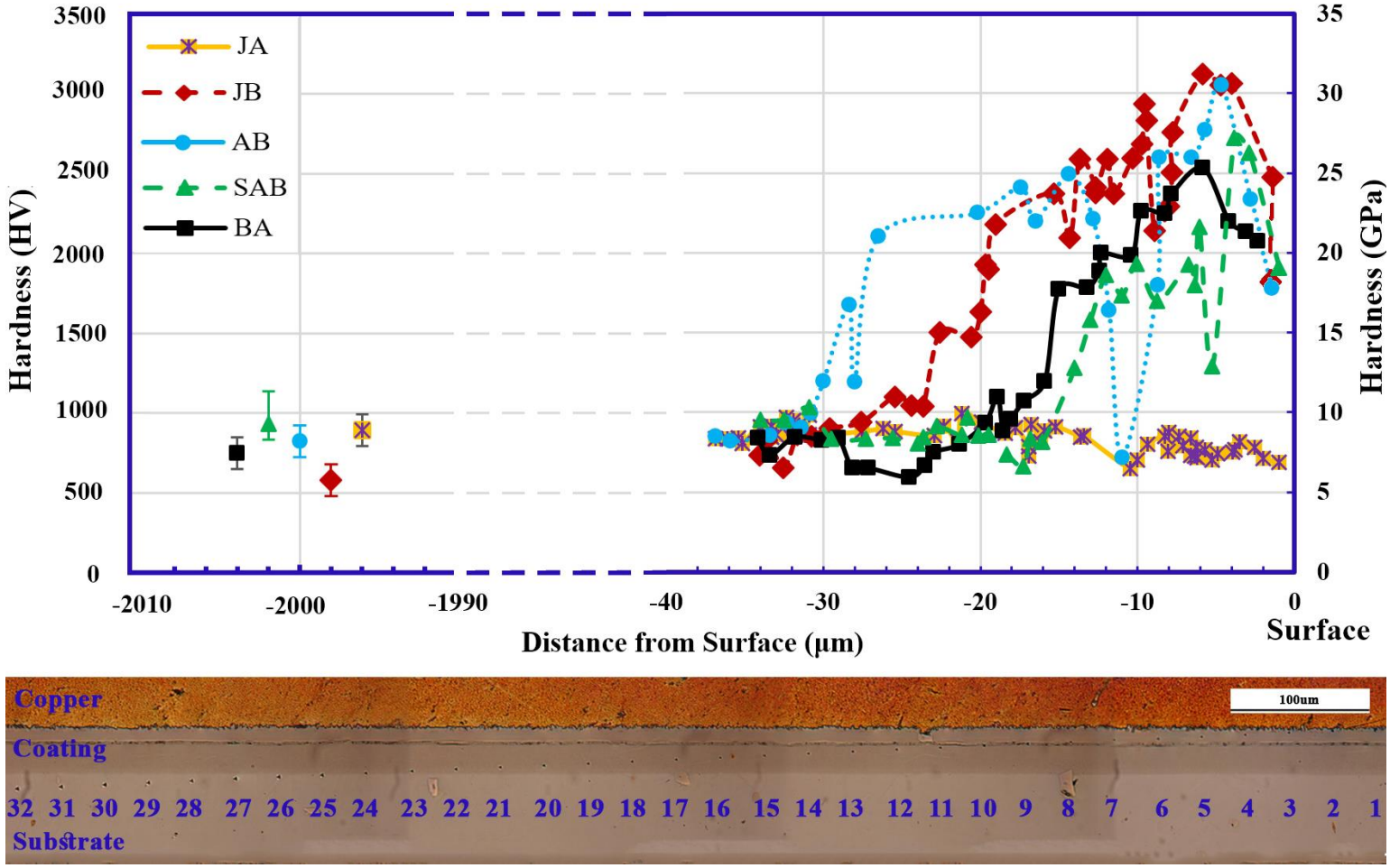


**Figure 4.11: Nano hardness profile of samples across the borided layer and in the bulk of the Inconel® 718 alloy. The error bars shown on the points in the left region of the graph are typical of the instrumental variability of the measured indentation.**

### 4.2.2 Microindentation Hardness

The nanoindentation hardness data, presented above, provide data on the fluctuations of hardness through the borided layer. The microindentation,Vickers, hardness data give a collective and complementary vision of the overall hardness of the boride layer and the bulk Inconel® 718 substrate alloy. Table 4.4 and Fig. 4.12 illustrate the Vickers hardness of the borided layer and substrate. The results confirm the findings of the nanoindentation hardness. Fig. 4.13 shows a typical Vickers hardness test that was done on the SAB sample. The size of the indentations illustrates the increased hardness of the coating compared to the substrate.

**Table 4.4: Vickers hardness of aged and/or borided coatings.**

| Hardness (VHN) / Condition | Coating | Interface | Bulk | Coating vs Substrate (%) |
|---|---|---|---|---|
| **JA** | - | - | 376 | - |
| **JB** | 1590.3 | 443.2 | 354.8 | 348 |
| **AB** | 1558.8 | 557.1 | 364 | 328.2 |
| **SAB** | 1526.5 | 449.1 | 381.4 | 300.2 |
| **BA** | 1169.3 | 478.3 | 373.2 | 213.3 |

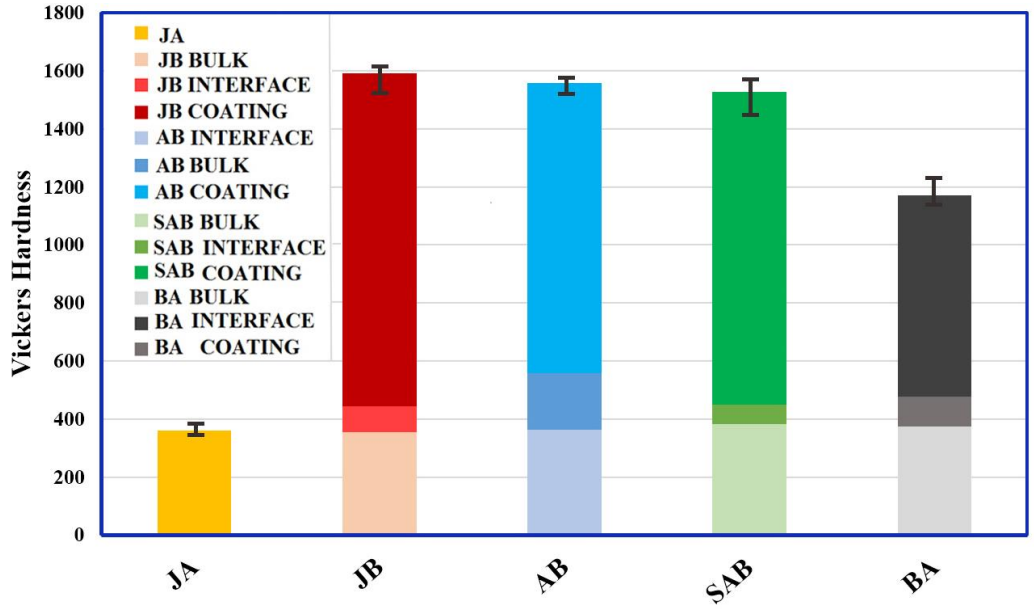


**Figure 4.12: Hardness of the coating, interface and substrate of samples from the JA, JB, AB, SAB, and BA conditions.**

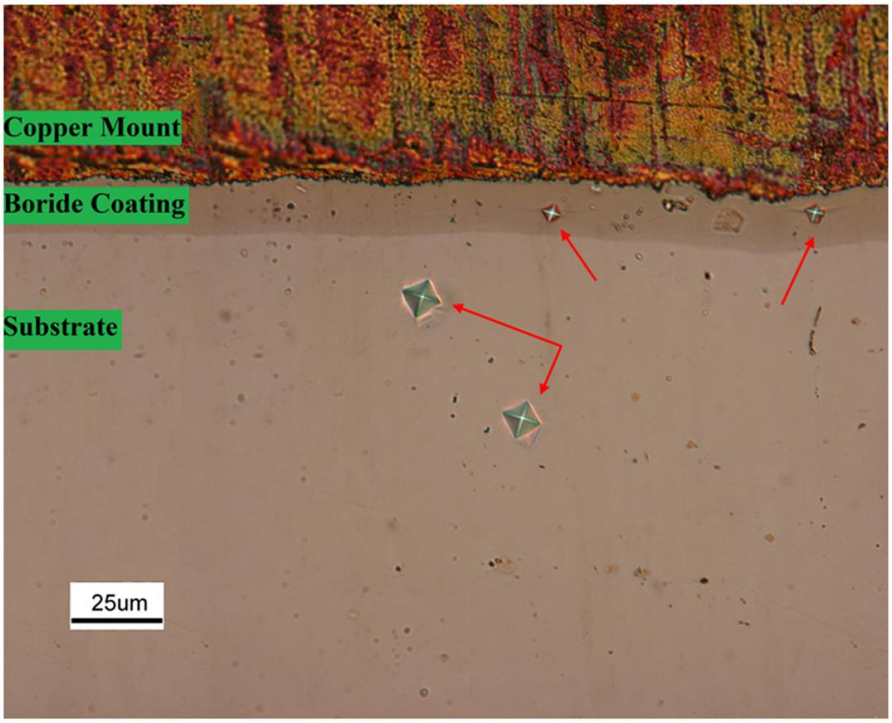


**Figure 4.13: Vickers hardness indentations performed on the SAB sample.**

## 4.3 Wear Properties of the Borided Samples

Scanning electron images of the wear track of the just aged (JA) Inconel® 718 alloy are shown in (Fig. 4.14) while those of the various borided samples are shown in Fig. 4.15. Wear tests were not done for the JB condition since surface properties of this condition were similar to the AB condition. The wear mechanism for JA sample is mostly adhesion wear. The JA pins showed net weight gain while the disc showed a net weight loss suggesting that, during the dry sliding, metal was being transferred, likely by a cold-welding process, from the disc to the pin. This appeared as debris on the pins that was visible with the unassisted eye.

Fig. 4.15 (e) and (f) reflect wear track in sample BA that is similar to AB in appearance. There is, still, significant amount of coating material on the surface while parts of its structure are torn off. Debris is available on the wear track and the mechanism of wear is abrasive wear. A detailed analysis of the topography of the worn pins from the various boride/aging conditions is given in Chapter 5.

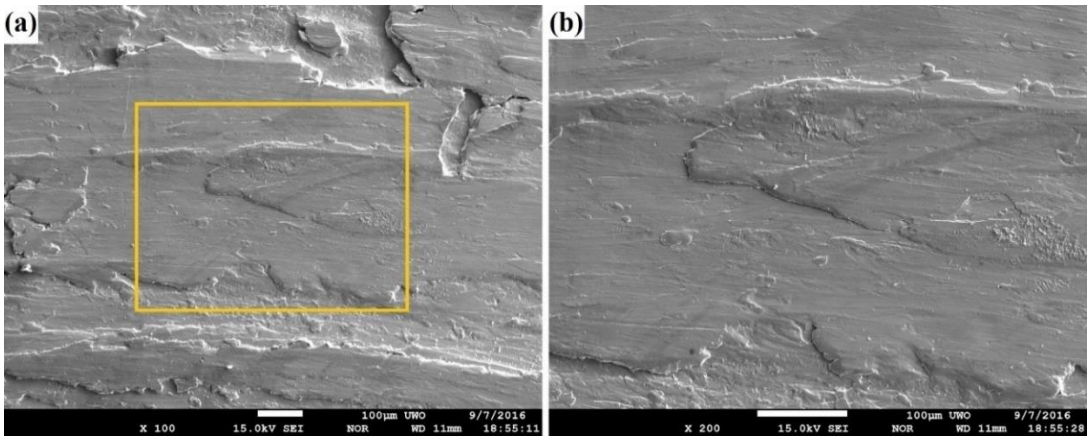


**Figure 4.14: Wear track of the Just Aged (JA) Inconel® 718 sample after 1000m with 4.7 MPa load at (a) 100X and (b) 200X.**

Fig. 4.16 shows the weight loss charts from the dry sliding wear tests performed at various average contact stress levels on the borided/aged Inconel® 718 samples. For all the conditions tested, the weight loss due to wear shows an approximately linear relationship with sliding distance. Table 4.5 lists the calculated average wear rate (mg/m) for the various wear tests performed.

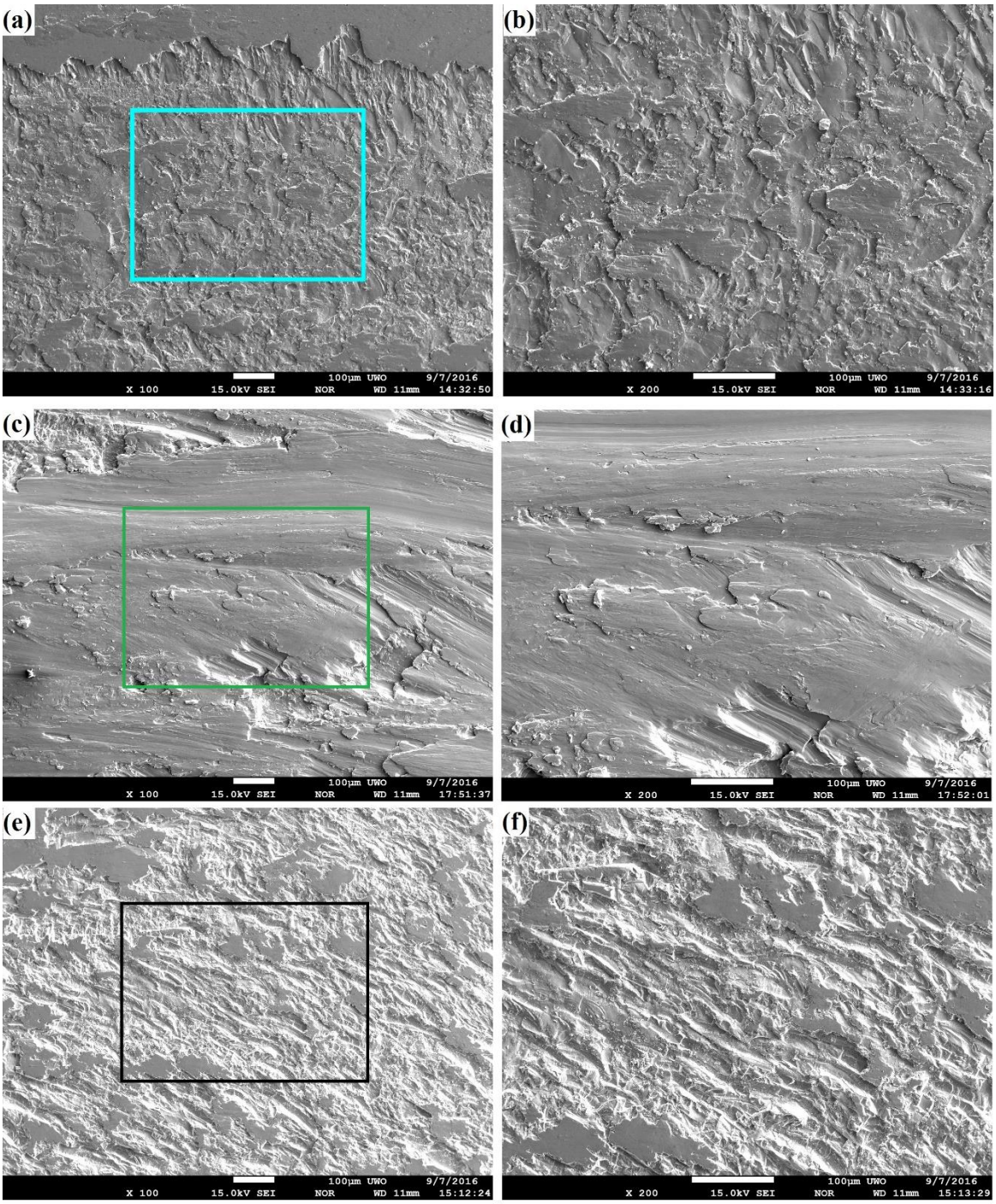


**Figure 4.15: Wear track of the borided Inconel® 718 samples after 1000m with 4.7 MPa load; (a) AB 100X; (b) AB 200X; (c) SAB 100X; (d) SAB 200X; (e) BA 100X; (f) BA 200X.**

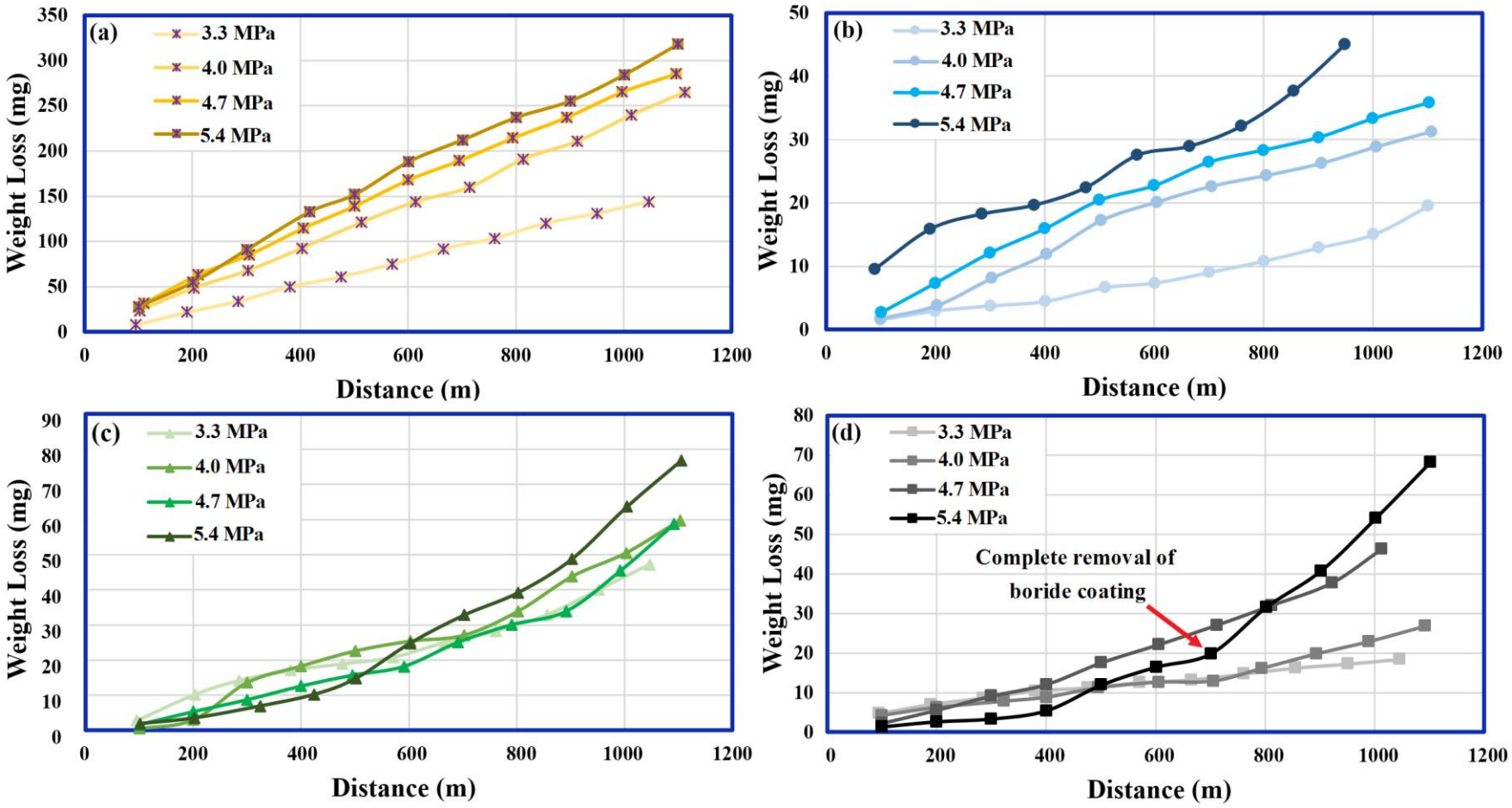


**Figure 4.16: Weight loss as a function of sliding distance when subjected to pin-on-disc dry sliding wear tests at various contact stress levels for samples of conditions (a) JA, (b) AB, (c) SAB and (d) BA.**

**Table 4.5: Calculated wear rate (mg/m) during the pin-on-disc dry sliding wear tests performed on Inconel® 718 samples subjected to various boride/aging conditions.**

| Condition | Weight loss slope at different loadings (mg/m) | | | |
|---|---|---|---|---|
| | 3.3 MPa | 4.0 MPa | 4.7 MPa | 5.4 MPa |
| **JA** | 0.15 | 0.22 | 0.23 | 0.24 |
| **AB** | 0.01 | 0.02 | 0.04 | 0.03 |
| **SAB** | 0.06 | 0.08 | 0.04 | 0.03 |
| **BA** | 0.01 | 0.01 | 0.04 | 0.03 |

# Chapter 5

# 5 DISCUSSION

The objective of this study was to determine the optimal method of boride surface hardening of age hardened Inconel® 718 alloy to produce a component that retains the high hardness of the age hardened substrate but provides improved wear resistance. The primary challenge in this study was to come up with a process whereby the thermal exposure necessary for boriding did not significantly decrease the hardness of the aged Inconel® 718. While the results of this study were presented in Chapter 4, what follows in this chapter is an analysis of the data resulting from the five boriding/aging treatments (AB, BA, SAB, JB, and JA).

Section 5.1 presents an analysis of the effect of the boriding treatments on the microstructure (topography, thickness, phases present, and chemical composition) of the boride layer.

Section 5.2 presents an analysis of the mechanical hardness of, and its variation across the thickness of the various boride layers and relates the local hardness to the microstructure.

Section 5.3 presents an analysis of the wear resistance, under high-stress dry-sliding conditions, of the various boride layers and relates the wear resistance to the microstructure.

## 5.1 Effect of Boriding and Aging Treatments on the Microstructure of the Boride Layer

### 5.1.1 Surface Roughness

The data (Table 4.1) show that the solution annealed Inconel® 718 in the polished condition has the lowest roughness. Aging the sample increases the roughness only slightly ($R_{rms}$ = 22 to 49 µm). The coating process, however, increases the roughness substantially, by a factor of about ten, and is the result of the diffusion and sintering of the Ekabor® Ni powders to the Inconel® 718 surface [7]. The roughness of the borided surface is a function of the temperature and time. As the temperature increases, more particles will undergo

premelting, attaching together or to the substrate and forming agglomerations thus increasing the roughness. prolonging the time at elevated temperature results in more complete diffusion of the surface agglomerates that decreases surface roughness. To illustrate this, the surface roughness of the SAB sample ($R_{rms}$ = 388 µm), which was borided at a low temperature and long time was significantly less than that of the JB and AB samples ($R_{rms}$ = 530 µm and 675 µm) that were boronized at a higher temperature for a shorter duration (Fig. 3.4).

According to the $R_{rms}$ surface roughness data (Table 4.1), BA shows relatively the highest roughness ($R_{rms}$ = 857 µm). However, the roughness profile of BA was different than the rest of the coating samples. While the surface profile of JB, AB and SAB was serrated, the profile of BA was sinusoidal with the transition from a peak to the next valley being very smooth and widely spaced.

The optical and SEM micrographs (Fig. 4.1, 4.2, 4.3 and 4.4) confirm the measured surface roughness data. The surface roughness has increased after boriding, but the topography of the BA is dissimilar. In the higher magnification (1000X) (Fig. 4.4 (a) and (b)), the granular and the gnarled structure is more obvious for JB and AB surfaces; it is less observable for SAB because it spent longer time at the processing temperature and this helped to smooth the agglomerations (Fig. 4.4 (c)). On the other hand, the BA structure is sponge-like, with no clear agglomerated features (Fig. 4.4 (d)). Upon first impression, one might attribute the unusual topography of the BA sample to be the result of the longer heat treatment (Fig. 3.4), helping to enhance the sintering process of the boride powders to the Inconel® 718 substrate. Further investigations, however, revealed that the reason is detachment of the top layers of the boride coating in the BA samples. This is discussed below.

### 5.1.2 Structure and Thickness of the Boride Layers

According to Fig. 4.6 and Table 4.2, the thickest boride layer was obtained for the JB and the AB samples. The mean thickness of the dispersed layer is 29.5 and 25.6 µm and the overall thickness is 54.0 and 58.4 µm for the JB and the AB samples respectively. The thickness of SAB stands at the other end of the list with the dispersed layer of only 15 µm and the overall layer of only 24.9 µm. The JB and AB samples were both borided at

800 ºC for 5 hours (Fig. 3.4), and thus their thickness is similar while in case of the SAB sample, although the aging and boronizing time (16 hours) was longer than JB and AB, the boronizing temperature (718 and 620 ºC) was considerably lower. The difference in coating thickness in these samples shows the dominating effect of boriding temperature versus boriding time, and is in agreement with diagrams in Fig 2.9 [2, 15].

The coating thickness in case of the BA sample is in contrast with the trends shown by the JB, AB, and SAB samples. The BA sample was first borided in 800 ºC for 5 hours; then, it was unpacked and aged in 718 and 620 ºC for 8 hours each; thus, it experienced longer exposure to elevated temperature than any of the other samples yet it contained a thinner boride layer (15.1 µm dispersed zone and 35.4 µm overall thickness) than the JB and AB samples (Fig. 4.6).

It was mentioned in the Section 4.1.2 that the coating layers in JB, AB and SAB conditions tend to crack. The nature of the cracks is straight and unbranched along the coating layer. Cracking of the top layer of boride coatings was a common problem during the sample preparation for the microstructure observations [49-50]. The BA samples however, displayed no cracking of the boride layer.

The unique differences observed with the boride layer of the BA sample compared to the other borided samples (JB and AB), namely, the smoother surface topography, the thinner boride layer, and the lack of visible cracks within the layer lead us to propose the following. There exist some levels of internal residual stress within all the boride layers which ends up making them susceptible to develop crack during either the coating process itself or during the sectioning and metallographic preparation process. In the case of the BA sample, its exposure to the extended aging process after the boriding process resulted in the cracked boride layer falling completely off during the aging process. This left only the lower portion of the boride layer still attached to the Inconel® 718 sample. This surface was smoother than the original borided surface. The remaining boride layer was, of course, thinner than the original layer but contained no internal cracks.

To validate this idea, the X-ray diffraction and the elemental analyses were pursued.

### 5.1.3 Chemical Composition of the Coating

It should be noted that X-ray diffraction method will provide crystal structure information from the top 10 μm of the sampled material. This means that the Bragg diffraction peaks obtained from the X-ray data performed on the borided surfaces from this study (Fig. 4.8) reflect the crystal phases present in both the compound zone and the dispersed zone of the coatings. The Just Borided (JB) sample had a coating layer composed of various types of nickel borides ($Ni_4B_3$, $Ni_3B$), nickel silicides ($Ni_3Si_2$, $Ni_3Si$) and iron borides (FeB, $Fe_2B$) (Fig. 4.8 (a)). Although the boriding process of the JB and AB samples was similar (5 hours in 800 $^oC$), the resulting phases were different. It is because the aging process in AB samples involved iron atoms in various types of precipitations like iron carbides that decreased their tendency to form iron boride compounds during following boronizing treatment; therefore, the iron boride phases were not detected. Accordingly, other combination of nickel borides and silicides ($Ni_4B_3$, $Ni_{4.6}Si_2B$) along with chromium boride ($Cr_2B_3$) were formed (Fig. 4.8 (b)).

For the SAB condition (Fig. 4.8 (c)), since the boriding temperature was lower than the other samples (718 $^oC$ and then 650 $^oC$ compare to 800 $^oC$), the boriding process was not active enough; thus, the resulting coating shows a lower proportion of boron/nickel or silicon/nickel compounds ($Ni_2B$, $Ni_2Si$, $CrNi_5Si_2$, $Ni_3Si$ and $CaNiSiO_6$). The boron/nickel ratio for the SAB samples is $\frac{1}{2}$ while this number is between $\frac{1}{3}$ to $\frac{3}{4}$ in case of JB and $\frac{3}{4}$ in case of AB. Similarly, the ratio of silicon/nickel is between $\frac{1}{3}$ and $\frac{1}{2}$ for SAB while this ratio is between $\frac{1}{3}$ to $\frac{3}{4}$ for JB, and $\frac{2}{4.6}$ for AB. Also, calcium compounds appear in the SAB condition but not in the other samples which were exposed to higher temperature.

For BA which spent longer time in high temperatures, the variety of borides and lack of silicide compounds is noticeable ($(Fe,Ni,Mo)_{23}B_6$, $Cr_2Ni_3B_6$, $Ni_{20}AlB_{14}$). As described before, it is speculated that, for this sample, the top layer of the BA coating was lost during the aging process. Thus, the acquired X-ray diffraction data is from the deeper part of the coating system that shows larger contribution from the alloying elements of the Inconel® 718 substrate in the boride compositions.

SEM WDS X-ray maps (Fig. 4.9) support the above mentioned XRD results. They clearly illustrate the boron contribution in the coating layer in the JB (Fig. 4.9 (b)), AB (Fig. 4.9 (c)), SAB (Fig. 4.9 (d)) and BA (Fig. 4.9 (e)) samples; on the other hand, the only sample that does not show silicon in its coating system is BA. The intensity of the silicon is highest on the very top layer of the coating for JB, AB and SAB (Fig. 4.9 (l), (m) and (n)). The presence of silicide layer in the coating structure confirms the existence of the silicide compounds in the Ekabor® Ni powder (Fig. 4.7).

Also, as mentioned before, a complete coating layer, like the ones in JB, AB and SAB samples, consists of three zones: (i) Compound Zone which is the top, thin (2-4 μm), silicide layer (mostly nickel silicide) (Fig. 4.10) whose observation by optic microscope is hard; (ii) Dispersed Zone composed of various metal borides that forms the main body of the coating, and (iii) Grain Boundary Zone that improves the coating adhesion to the substrate (Fig. 4.6). This observation of three-zone structure of the borided surface layer is consistent with that reported earlier by Matsuda *et al.* (Fig. 2.7)) [34]. The only difference is the top silicide layer being thin in the obtained coatings of this study on account of the fact that the amount of silicon compounds is lower in our boriding powder (Ekabor® Ni). A thin silicide layer leads to further diffusion of boron into the substrate that could cause partial brittleness and cracking (Fig. 4.5).

The maps for other elements (Fig. 4.10) suggest that little chromium and iron is present, while nickel and silicon are abundant, in the top part of the boride layer. The difference between the nickel concentration at the top layer (80%) and the substrate suggests that the dominant nickel resource forming the external silicide layer is from Ekabor® Ni powder which contains $Ni_2O_3$ within its mixture (Fig. 4.7).

In contrast, no high intensity silicon region could be distinguished in the BA sample. Fig. 4.9 (o) is in agreement with Fig. 4.8 (d) results showing no silicon trace within the first 10 μm of the coating surface; this is another supporting clue for the separation of the top layer in BA coating that has occurred during the post-boronizing aging treatment.

According to the SEM WDS point analyses, the top part of the coating layer, where the silicides were dominant, contained 9.6% Si for JB, 14% Si for AB and 7.6% Si for SAB.

The lower amount of the silicon in the SAB sample is probably because of the lower boriding/aging temperature. Below the silicide layer, the amount of boron is about the same (16% to 17.7%) in JB, AB and SAB, but the thickness of SAB is less and this is another effect of the lower boriding temperature for this sample. Point analysis data for BA sample shows no silicon amount and lower amount of boron (10%) at the top layer while the boron amount remains constant within some depths of the coating. Less amount of boron in the BA coating is because of separation of the top layer; besides, these samples spent more time at high temperature delivering more uniform distribution of boron within the coating layer.

In summary, the reason behind the crack formation in boride layer is attributed to excessive boron diffusion, segregation of alloying elements within the layer, formation of various kinds of boride and silicide compounds with dissimilar crystal structures and thermal expansion coefficients that accumulates considerable amount of residual stress within the coating layer.

## 5.2 Effect of Boride Layer Microstructure on the Hardness of the Boride Layer

### 5.2.1 Nanoindentation Hardness

Based on the nano hardness results in Fig. 4.11, the hardness within the first 25 µm of the borided/aged Inconel® 718 samples is between 20 to 31 GPa. That is 230% to 350% increase compared to the Just Aged (JA) Inconel® 718 material.

Since the coating is composed of various silicide and boride compounds with different hardnesses, and the indentations are in micron size, about 300 nm in depth and about 1200 nm in diagonal length, the hardness profile shows considerable fluctuation within the coating layer. A couple of indentations were omitted from the beginning of the chart in order to neglect the edge effect. For JB, AB and SAB the hardness of the coating at 2 µm from the edge is about 16 GPa; this is the zone where the silicide compounds are dominant (Fig. 4.9); thus, the top silicide layer shows a higher hardness than the Inconel® 718 substrate but lower hardness than the boride compounds. Moving through the boride layer the hardness raises sharply to about 30 GPa. The high hardness of these samples

corresponds with the beginning of boride compounds at a depth of about 5 μm into the layer. The amount of boron at this point is about 16.0% (JB), 17.7% (AB) and 17.5% (SAB). At the region of the boride layer that contains the long central cracks the hardness drops considerably, possibly due to the presence of the crack resulting in a loss of lateral constraint during the indentation process, but elevates again to about 29.4 GPa (JB), 24.9 GPa (AB) and 21.6 GPa (SAB). This finding shows that the crack was developed within the most hardened section of the coating. After that, the hardness drops with increasing distance through the boride layer to about 11 GPa (the characteristic nanohardness of the aged Inconel® 718 substrate). If we define the "effective thickness" as the boride layer thickness over which the nanoindentation hardness is significantly higher than that of the substrate metal, we see that the effective thickness is close in magnitude to the measured thickness of the dispersed zone (Table 4.2).

The BA sample showed significantly different nanohardness profile through the boride layer compared to the other samples. Its hardness profile was generally smoother and less serrated. We attribute this to the more uniform boron distribution through the boride layer of the BA sample despite the fact that the boron concentration was less (about 10% B) than the other samples (16.0% (JB), 17.7% (AB) and 17.5% (SAB)). Since the boron concentration is less, the hardness of the boronized layer in the BA sample is also less compare to the rest of the samples.

The average hardness of the substrate shows that the JB samples have the lowest hardness (5.8 GPa) which is related to the absence of γ" precipitations since the age hardening was not accomplished on them. On the other hand, JA and SAB acquired the maximum hardness in the bulk of the material, 8.9 and 9.4 GPa respectively, which shows that the aging was influential in improving the hardness. The hardnesses of AB (8.2 GPa) and BA (7.5 GPa) are ranked in between; since they have experienced an extra heat treatment before or after the aging, the lower hardness could be attributed to the excessive growth of the hardening precipitations like γ' and γ". The hardness of AB and BA, as a result, shows a decrease of about 7.9% and 15.7% with respect to JA condition.

### 5.2.2 Microindentation Hardness

The micro indentation hardness data (Table 4.4 and Fig. 4.12) shows the same general trends as the nano indentation tests. As depicted in Fig. 4.12, the hardnesses of JB and AB are highest with 1590 and 1558.8 HV. The BA coating has the lowest hardness (1169.3 HV).

Using Eq. 2.4 [34], the estimated Vickers hardness of the boride layer should be around 1935.1 HV while our results show a hardness range between 1169 to 1590 HV; that is an overestimation of about 345 to 766 HV. Consequently, similar to other commercial nickel alloys, this equation fails to predict the exact hardness of Inconel® 718 as well.

The hardness “at the interface” refers to the tests that were done in the lower region of the boride layer where the boride precipitates occur along pre-existing grain boundaries of the Inconel® 718. The hardness at this region is between 443.2 to 557.1 HV. The presence of this grain boundary zone provides a gradual transition in hardness between the dispersed zone and the substrate that enhance the bonding between the coating and the substrate.

The hardness of the substrate is consistent with the nano hardness test results. The JA and SAB, whose heat treatments were similar, show the highest hardness, 381.4 and 376 HV. This amount is a little bit less than the claimed hardness in the supplier’s datasheet (~ 425 HV). The lowest hardness (354.8HV) belongs to the sample JB which was not aged; thus, it is assumed that the microstructure in JB lacks the hardening precipitations like γ".

The measured hardnesses of Vickers tests are more uniform in view of the fact that the indentations in this method involve a considerable amount of material in hardness test and the applied force is much higher. Thus, the hardness measured by these two methods are not comparable (Table 4.2 and Table 4.4).

## 5.3 Effect of the Boride Layer on the Wear Resistance

As described in section 3.2.5, the pin-on-disc dry sliding wear tests were performed at four stress levels (3.3, 4.0, 4.7 and 5.4 MPa) over a total sliding distance of 1000 m. Since only one test was performed in each loading condition, the repeatability and tolerance of

observed trend could not be confirmed; these tests, however, provide significant information.

Fig. 4.16 shows an approximate linear relationship between weight loss and the wear distance. For the sample JA (Fig. 4.16 (a) and Table 4.5), which did not have a coating, the wear rate increases by increasing the loading level; for example, the slope of the weight loss versus the sliding distance increases sharply from 0.15 to 0.22 mg/m when the contact stress increases from 3.3 to 4.0 MPa. However, no specific mathematical relationship exists between weight loss rate and loading level.

By comparing the amount of the wear loss between JA condition with borided ones, it is apparent that the boride coating decreased the metal loss during dry sliding wear. As a case in point, after 800 m sliding distance at a contact stress of 3.3 MPa, the percentage of the weight loss for the coated samples is 10 to 25% of the unborided sample. Among the borided samples, the best wear resistance belongs to the AB sample while the worst belongs to SAB. The performance for the borided samples during dry sliding at higher stress levels (4.7 MPa) is even better with only 14% of the weight loss of the unborided sample. This is because when the load increases, the wear rate increase in case of JA is much higher than the ones for borided samples.

All the samples display nearly linear weight loss versus sliding distance characteristics. While the AB and BA samples display the lowest wear rates under high stress (4.7 MPa) dry sliding conditions, all the borided samples (AB, BA and SAB) demonstrate nearly similar wear properties. That means the types of the borides formed in the different conditions (Fig. 4.8) did not affect the wear performance. At this high stress level the amount of wear loss begins to rise fast for the SAB and BA samples in the last cycle of the test (after a sliding distance of about 900 m).

In highest stress level (5.4 MPa), the coating in all the samples were worn and the wear loss amount has increased in last cycles of all the conditions. Accordingly, the thinnest coat (SAB) was worn before than thicker ones (BA and SAB).

SEM images of the worn surfaces after 1000 m sliding distance at 4.7 MPa stress are shown in Fig. 4.14 and Fig. 4.15. As mentioned before the sample JA underwent severe plastic deformation and adhesion wear. The wear traces of the AB sample (Fig. 4.15 (a) and (b)) do not show signs of plastic deformation; instead, pieces of coating are torn out leaving a flake-like structure on the wear track and debris is visible that is embedded within the wear track. This suggests an abrasive wear mechansim. In this sample a significant portion of the boride coating layer is still present after 1000 m dry sliding distance at 4.7 MPa contact stress. This indicates that the boride compounds present in the boride layer have very high resistance to loading conditions associated with sliding abrasive wear.

The SAB sample (Fig. 4.15 (c) and (d)) wear surface is more similar to that of the uncoated Inconel® 718, inasmuch as the dispersed layer of the coating system was exhausted completely after 1000 m sliding at a contact stress of 4.7 MPa. The wear traces on the SAB and the JA samples show features characteristic of considerable plastic deformation while in the case of the SAB sample, some boride fragment wear debris was still remaining. Thus, the wear mechanism in the SAB sample, is a mixture of abrasive and adhesive wear.

Finally, Fig. 4.15 (e) and (f) indicates the wear track of the BA sample. In sample BA, the wear surface is similar to AB where a considerable amount of coating material remained on the surface, but some parts were removed. The wear mechanism in this case is also abrasive.

Hence, the coating layer has modified the wear mechanism from adhesive in unborided Inconel® 718 to abrasive in borided ones, and the adhesive wear remains as the prevailing mechanism (like AB and BA at 4.7 MPa) until the coating is consumed (like SAB at 4.7 MPa).

These wear results present an interesting finding; namely, that the presence of the long cracks in the mid-thickness regions of the boride layers did not detract from their wear resistance. No sudden weight loss was recorded during the sliding wear tests and this signifies that the coating did not spall off suddenly during the course of testing even though our metallographic analyses indicate that they are susceptible to cracking. A reason that cracking did not affect the sliding wear resistance may be that the applied compressive

stresses between the pin and the disc during these tests tend to constrain the cracked boride layer and prevent its further detachment during sliding shear.

To conclude, although the amount of boron within the coating layer is important, the factor that increases the wear resistance of the borided coatings is their thickness. The sample AB, with its highest boride layer thickness, offers the lowest wear rate of all the conditions tested.

# Chapter 6

# 6 CONCLUSION AND FUTURE WORK

Boriding of the age hardened nickel-based alloy Inconel® 718 was studied to determine the optimal method for applying a high hardness, wear resistance nickel boride surface layer onto this alloy without compromising the alloy's age hardening. Five aging/boriding thermal conditions were studied: Just Boriding (JB); Aging and then Boriding (AB); Simultaneous Aging and Boriding (SAB); Boriding and then Aging (BA), and Just Aging (JA). Our evaluating criteria was the microstructure of the coating and substrate as well as their hardness and wear resistance.

Roughness evaluation shows that the roughness of the coatings are more than uncoated sample, and with increasing of coating thickness the roughness has increased. Samples JB, AB and SAB had similar roughness profile while BA profile was more unlevel but with less frequency. Moreover, coating thickness of BA was less than the rest of the samples and lacked the top silicide layer on its structure which is typical of boride coatings. All these evidence together signifies that a part of boride layer was broken and removed during aging in case of BA due to residual stresses and varied coefficient of expansion.

The microstructure of the coating shows that it comprises of different layers: a top silicate layer (2-4 μm) (compound zone), an intermediate dispersed zone composed of boride compounds (11-25 μm), and a grain boundary zone (9-32 μm) which is the result of fast boron diffusion along the grain boundary area. Composition studies also show various forms of borides like $Ni_2B$, NiB and $Ni_3B_4$ that are responsible for hardness in coating.

The hardness of the substrate shows that boriding has a negligible effect on the hardness. Therefore, it could be concluded that the microstructural features have not transformed during the boride process. The hardness of the boride layer (~1500 HV) was more than three times higher than the core of the samples (~380 HV) and wear tests reflected that the protection against abrasion has improved over 80%. Although the hardness of samples was partially different and some of the conditions were prone to develop crack within the layer, all the coating systems were successful to effectively decrease the wear damage.

Other than above mentioned results, the determining factor for coating efficiency is its thickness. That means whichever coating that is thicker could resist the wear better. The results shows that AB and JB have the thickest coating layer among the considered conditions. JB, nonetheless, has less hardness of the substrate since it did not undergo standard aging heat treatment. The hardness of substrate in AB, also, does not show considerable drop after boronizing (less than 8%); that is, the microstructure of the substrate was not affected by 5 hours of boronizing at 800 $^{o}$C. Therefore, among the nominated recipes for this project, Aging and Boronizing (AB) is the most effective. This type of procedure is best accomplished by:

- ✓ Aging for 8 hours at 718 $^{o}$C at vacuum furnace;
- ✓ Cooling down to 620 $^{o}$C with 100 $^{o}$C/per hour;
- ✓ Holding at 620 $^{o}$C for 8 hours at vacuum furnace;
- ✓ Air cooling to room temperature;
- ✓ Boronizing at a pack containing Ekbor Ni powder at 800 $^{o}$C for 5 hours at controlled atmosphere like argon;
- ✓ Cooling down at air.

Nevertheless, there are some issues that should be focused on for further studies. As a case in point, the susceptibility of the boride layers to cracking should be studied further in order to understand whether there will be problem in long term or not. Another complementary part of this topic is to do a comparison between the results of this study with a sample that undergoes boriding first; then, solution annealing and aging to know whether it is possible to retain the mechanical properties of substrate even more.

# References


[1] M. J. Donachie and S. J. Donachie, Superalloy: A Technical Guide, 2nd ed. 2002.

[2] D. Mu, B. Luo Shen, C. Yang, and X. Zhao, "Microstructure Analysis of Boronized Pure Nickel using Boronizing Powders with SiC as Diluent," Vacuum, vol. 83, no. 12, pp. 1481–1484, 2009.

[3] A.S.T.M. (A1014-03), Standard Specification for Precipitation-Hardening Bolting Material (UNS N07718) for High Temperature Service. 2003.

[4] S.A.E. (A. M. S. 5663M), Nickel Alloy, Corrosion and Heat-Resistant, Bars, Forgings, and Rings 52.5Ni - 19Cr - 3.0Mo - 5.1 Cb (Nb) - 0.90Ti - 0.50Al - 18Fe Consumable Electrode or Vacuum Induction Melted 1775 ºF (968 ºC) Solution and Precipitation Heat Treated. 2004.

[5] "Special Metals." [Online]. Available: http://www.specialmetals.com/documents/Inconel alloy 718.pdf.

[6] D. Hasan, M. Amir, and C. Huseyin, "Thermochemical Boriding of Inconel 718 Superalloy," Acad. J. Sci., vol. 2165–6582, no. 9, pp. 382–389, 2013.

[7] M. Aliofkhazraei, Superalloys. 2015.

[8] A. Oradei-Basile and J. F. Radavich, "A Current T-T-T Diagram for Wrought Alloy 718," Superalloys 718, 625 Var. Deriv., pp. 325–335, 1991.

[9] A.S.T.M., "B 637 - 06: Standard Specification for Precipitation-Hardening Nickel Alloy Bars, Forgings, and Forging Stock for High- Temperature Service," pp. 1–8, 2003.

[10] A.S.M., A.S.M. Handbook Volume 4: Heat Treating. 1994.

[11] B. Geddes, H. Leon, and X. Huang, Superalloys: Alloying and Performance. ASM International, 2010.

[12] X. You, Y. Tan, S. Shi, J.-M. Yang, Y. Wang, J. Li, and Q. You, "Effect of Solution Heat Treatment on the Precipitation Behavior and Strengthening Mechanisms of Electron Beam Smelted Inconel 718 Superalloy," Mater. Sci. Eng. A, vol. 689, no. 2, pp. 257–268, 2017.

[13] H. K. D. H. Bhadeshia, "Nickel and Nickel Based Superalloys," University of Cambridge, 2003. [Online]. Available: http://www.msm.cam.ac.uk/phase-trans/2003/Superalloys/superalloys.html.

[14] G. E. Korth and C. L. Trybus, "Tensile Properties and Microstructure of Alloy 718 Thermally Aged to 50,000 Hours," Superalloys 718, 625 Var. Deriv., pp. 437–446, 1991.

[15] N. Ueda, T. Mizukoshi, K. Demizu, T. Sone, A. Ikenaga, and M. Kawamoto, "Boriding of Nickel by the Powder-Pack Method," Surf. Coatings Technol., vol. 126, no. 1, pp. 25–30, 2000.

[16] A. Naji, M. C. Galetz, and M. Schutze, "Design Model for Diffusion Coatings Formed via Pack Cementation," Mater. Corros., vol. 65, no. 3, pp. 312–318, 2014.

[17] V. Sista, O. Kahvecioglu, G. Kartal, Q. Z. Zeng, J. H. Kim, O. L. Eryilmaz, and A. Erdemir, "Evaluation of Electrochemical Boriding of Inconel 600," Surf. Coatings Technol., vol. 215, pp. 452–459, 2013.

[18] D. Curtis, "Case hardening nickel alloys," Mater. Des., vol. 14, no. 6, pp. 349–350, 1993.

[19] J. A. Sue and T. P. Chang, "Friction and Wear Behavior of Titanium Nitride, Zirconium Nitride and Chromium Nitride Coatings at Elevated Temperatures," Surf. Coatings Technol., vol. 76–77, pp. 61–69, 1995.

[20] J. A. Sue and H. H. Troue, "High Temperature Erosion Behavior of Titanium Nitride and Zirconium Nitride Coatings," Surf. Coatings Technol., vol. 49, no. 1–3, pp. 31–39, 1991.

[21] E. Martinez, J. Romero, A. Lousa, and J. Esteve, "Wear Behavior of Nanometric CrN/Cr Multilayers," Surf. Coatings Technol., vol. 163–164, pp. 571–577, 2003.

[22] L. Major, J. Morgiel, B. Major, J. M. Lackner, W. Waldhauser, R. Ebner, L. Nistor, and G. Van Tendeloo, "Crystallographic Aspects Related to Advanced Tribological Multilayers of Cr/CrN and Ti/TiN Types Produced by Pulsed Laser Deposition (PLD)," Surf. Coatings Technol., vol. 200, no. 22–23 SPEC. ISS., pp. 6190–6195, 2006.
[23] F. Cai, "Tribological and Electrochemical Corrosion Behavior of Titanium Nitride and Chromium Nitride Based PVD Coating Systems," 2011.
[24] M. Naveed, A. Obrosov, and S. Weiß, "Investigation of the Wear Resistance Properties of Cr / CrN Multilayer Coatings against Sand Erosion," Eur. Symp. Frict. Wear, Wear Prot., vol. 2015, p. 10, 2014.
[25] N. Makuch, M. Kulka, and A. Piasecki, "The Effects of Chemical Composition of Nimonic 80A-Alloy on the Microstructure and Properties of Gas-Borided Layer," Surf. Coatings Technol., vol. 276, pp. 440–455, 2015.
[26] H. Aytekin and Y. Akçin, "Characterization of Borided Incoloy 825 Alloy," Mater. Des., vol. 50, pp. 515–521, 2013.
[27] M. Keddam and S. M. Chentouf, "A Diffusion Model for Describing the Bilayer Growth (FeB / Fe 2 B) during the Iron Powder-Pack Boriding," vol. 252, pp. 393–399, 2005.
[28] M. Baydogan and S. I. Akray, "Successive Boronizing and Austempering for GGG-40 Grade Ductile Iron," J. Iron Steel Res. Int., vol. 16, no. 2, pp. 50–54, 2009.
[29] L. G. Yu, K. A. Khor, and G. Sundararajan, "Boriding of Mild Steel Using the Spark Plasma Sintering (SPS) Technique," Surf. Coatings Technol., vol. 157, no. 2–3, pp. 226–230, 2002.
[30] "BorTec GmbH & Co.KG." [Online]. Available: http://www.bortec.de/unternehmen/?lang=en.
[31] G. Palombarini and M. Carbucicchio, "Influence of Carbon on the Chromium Redistribution when Boriding Iron Alloys," J. Mater. Sci. Lett., vol. 12, pp. 797–798, 1993.
[32] I. Gunes, "Wear Behavior of Plasma Paste Boronized of AISI 8620 Steel with Borax and B2O3 Paste Mixtures," J. Mater. Sci. Technol., vol. 29, no. 7, pp. 662–668, 2013.
[33] I. Ozbeka, H. Akbulut, S. Zeytin, C. Bindal, and A. H. Ucisikb, "The Characterization of Borided 99.5 % Purity Nickel," Surf. Coat. Technol., vol. 126, pp. 166–170, 2000.
[34] F. Matsuda, K. Nakata, and Y. Nishio, "Surface Hardening of Ni-base Alloys with Boronizing Technique," Trans. JWRI, vol. 16, no. 145–157, 1987.
[35] O. Torun and I. Çelikyürek, "Boriding of Diffusion Bonded Joints of Pure Nickel to Commercially Pure Titanium," Mater. Des., vol. 30, pp. 1830–1834, 2009.
[36] D. W. Deng, C.-G. Wang, Q.-Q. Liu, and T.-T. Niu, "Effect of Standard Heat Treatment on Microstructure and Properties of Borided Inconel 718," Trans. Nonferrous Met. Soc. China (English Ed., vol. 25, no. 2, pp. 437–443, 2015.
[37] M. Kulka, P. Dziarski, N. Makuch, A. Piasecki, and A. Miklaszewski, "Microstructure and Properties of Laser-Borided Inconel 600-Alloy," Appl. Surf. Sci., vol. 284, pp. 757–771, 2013.
[38] V. Vitry, "Electroless Nickel-Boron Deposits: Synthesis, Formation and Characterization; Effect of Heat treatments; Analytical Modeling of the Structural State," 2009.
[39] H. Baker, Ed., ASM Handbook: Volume 3, Alloy Phase Diagrams. A.S.M., 1992.
[40] I. Jauhari, H. A. M. Yusof, and R. Saidan, "Superplastic Boronizing of Duplex Stainless Steel under Dual Compression Method," Mater. Sci. Eng. A, vol. 528, no. 28, pp. 8106–8110, 2011.
[41] H. Rajakumar, "Thermal Kinetics of Ion Irradiation Hardening in Selected Alloys for the Canadian Gen. IV Nuclear Reactor Concept," University of Western Ontario, 2015.
[42] A.S.T.M. E 407-99, "Standard Practice for Microetching Metals and Alloys," A.S.T.M., pp. 1–22, 1999.

[43] A.S.T.M. E112-12, “Standard Test Methods for Determining Average Grain Size,” ASTM, pp. 1–27, 2012.
[44] W. C. Oliver and G. M. Pharr, “An Improved Technique for Determining Hardness and Elastic Modulus using Load and Displacement Sensing Indentation Experiments,” J. Mater. Res., vol. 7, no. 6, pp. 1564–1583, 1992.
[45] W. C. Oliver and G. M. Pharr, “Measurement of Hardness and Elastic Modulus by Instrumented Indentation: Advances in Understanding and Refinements to Methodology,” J. Mater. Res., vol. 19, no. 1, pp. 3–20, 2004.
[46] D. Tabor, The Hardness of Metals. Oxford Classic Texts in the Physical Science, 2000.
[47] A.S.T.M. E 384-05 A, “Standard Test Method for Microindentation Hardness of Materials,” pp. 1–24, 2002.
[48] http://tribolab.mas.bg.ac.rs/english/images/equipment/T-62_jpg, University of Belgrade, Tribolab, 2008.
[49] T. W. Spence and M. M. Makhlouf, “Characterization of the Operative Mechanism in Potassium Fluoborate Activated Pack Boriding of Steels,” J. Mater. Process. Technol., vol. 168, pp. 127–136, 2005.
[50] I. Uslu, H. Comert, M. Ipek, F. G. Celebi, O. Ozdemir, and C. Bindal, “Evaluation of Borides Formed on AISI P20 Steel,” Mater. Des., vol. 28, pp. 55–61, 2007.

# Curriculum Vitae

## ARIA KHALILI

### Academic Achievements

Master of Science — Sep. 2005- July 2008
Azad University, Science & Research Branch, Tehran, Iran

Bachelor of Science — Sep. 2000- Jan. 2005
Azad University, Science & Research Branch, Tehran, Iran

### Teaching Professional Development

Teaching Assistant, "Materials Engineering" — Fall 2015 &Winter 2016

Teaching Assistant, "Energy Conversion" — Jan. 2015

### Selective Publication(s)

Journal Paper (s):

"On room-temperature Nanoindentation Response of an Al-Li-Cu alloy" — Aug. 2016
M. Haghshenas, A. Khalili, R. Ranganathan (Materials Science and Engineering A)

"Nano Mechanical Behaviour and Microstructure of Boride Layers Formed on Inconel 718 Before and After Aging" — Oct. 2016
A. Khalili, R. J. Klassen, Materials Science & Technology (MS&T16) (Proceeding).

Conference Paper(s):

"Microstructure and Microhardness of Boride Layers Formed on Inconel 718 Before, During, and After Aging" — June 2016
A. Khalili, R. J. Klassen, Canadian Materials Science Conference (CMSC), Mc Master, Hamilton, ON

"Effect of Irradiation on Mechanical Properties of Inconel X-750" — Dec. 2015
A. Khalili, F. Nie, R. J. Klassen, The University Network of Excellence in Nuclear Engineering (UNENE), Mississauga, ON.

"Effect of SDS and Saccharine on Ni-SiC Composite Coatings Electrodeposition" — Aug. 2010
A. Khalili, A. Afshar, International Conference on Nanotechnology: Fundamentals and Applications, Ottawa, ON.

### Patent(s)

Process of Electroplating of Ni- SiC Composite Coating — 2008
A. Khalili, A. Afshar, Iran Patents# 900504.

### Honors, Awards and Grants

Western Graduate Research Scholarship (W.G.R.S.) — Jan. 2015- Dec. 2016
School of Graduate and Postdoctoral Studies, University of Western Ontario,